THE ROYAL SOCIETY

Unusual crystal structures and properties of nitronylnitroxide radicals. Possible RVB states in molecule-based magnets

By Kunio Awaga[1,2], Nobuo Wada[1], Isao Watanabe[3] and Tamotsu Inabe[4]

[1]*Department of Basic Science, Graduate School of Arts and Sciences, The University of Tokyo, Komaba, Meguro, Tokyo 153-8902, Japan*
[2]*PRESTO, Japan Science and Technology Corporation, Kudan-Minami, Chiyoda, Tokyo 102-0074, Japan*
[3]*Muon Science Laboratory, The Institute of Physical and Chemical Research (RIKEN), Hirosawa, Wako, Saitama 351-0198, Japan*
[4]*Division of Chemistry, Graduate School of Science, Hokkaido University, Sapporo 060-0810, Japan*

We studied two kinds of novel low-dimensional magnetic systems found in the crystals of nitronylnitroxide molecular compounds: Kagome lattice and spin ladder. (i) In the crystals of *m*-MPYNN · X (*m*-MPYNN is *m*-*N*-methylpyridinium nitronylnitroxide and X = I, BF_4, ClO_4, etc.), *m*-MPYNN ($S = 1/2$) exists as a ferromagnetic dimer and the dimers form a triangular lattice with a weak interdimer antiferromagnetic coupling that brings about spin frustration. The magnetic system can be regarded as a spin-1 Kagome antiferromagnet at low temperatures. The low-temperature magnetic measurements revealed a spin-gap ground state, which was possibly identical with the RVB state. The temperature dependence of the heat capacity did not show long-range magnetic ordering down to 0.1 K, but short-range ordering caused by the interdimer interaction. The μ^+SR exhibited the temperature-independent depolarization behaviour down to 30 mK, supporting no long-range ordering and a non-magnetic ground state. By replacing the *N*-methyl group in *m*-MPYNN with longer alkyl chains, slightly distorted Kagome lattices were obtained, in which the spin gap state collapsed. (ii) The crystal of *p*-EPYNN · $[Ni(dmit)_2]$ (*p*-EPYNN is *p*-*N*-ethylpyridinium nitronylnitroxide and $[Ni(dmit)_2]$ is nickel bis(4,5-dithiolato-1,3-dithiole-2-thione)) includes a ladder structure of $[Ni(dmit)_2]$ ($S = 1/2$) sandwiched by ferromagnetic chains of *p*-EPYNN ($S = 1/2$). The magnetic measurements clearly demonstrated a spin gap of *ca.* 1000 K for the molecular spin ladder. Impurity effects on the ladder were studied by making a solid solution system, *p*-EPYNN · $[Ni(dmit)_2]_{1-x} \cdot [Au(dmit)_2]_x$ with $0 \leqslant x \leqslant 0.5$. The doping of the non-magnetic $[Au(dmit)_2]$ increased Curie defects in the ladder, and resulted in antiferromagnetic behaviour of *p*-EPYNN at low temperatures.

Keywords: Kagome antiferromagnet; spin ladder; nitronylnitroxide; spin gap

1. Introduction

Magnetic properties of a large number of transition metal complexes, organic radicals and metal–organic radical complexes have been studied so far, and the search for

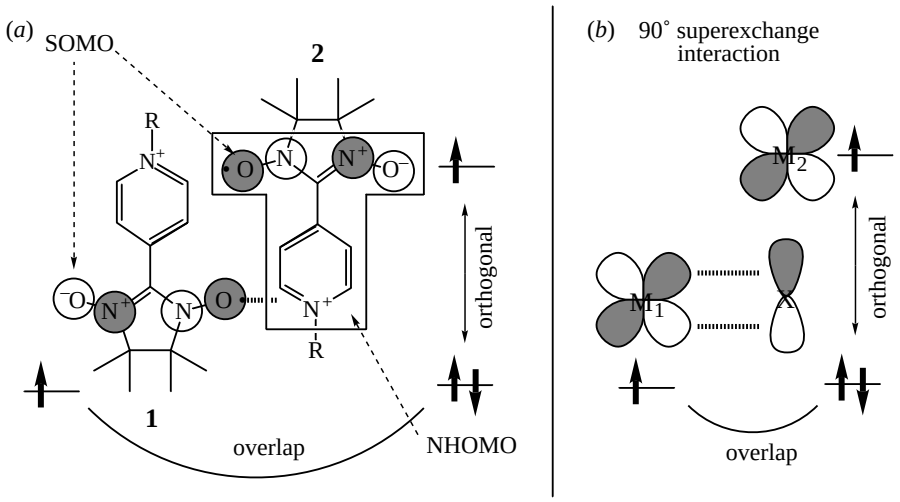

Scheme 1.

molecule-based magnetic materials has intensified in recent years (Day 1993). In this field, a stable organic radical family, nitronylnitroxide, has attracted much interest, because of potential ferromagnetic properties. Various nitronylnitroxide derivatives have been found to exhibit ferromagnetic intermolecular interactions in their bulk crystals (Awaga & Maruyama 1989; Wang *et al*. 1993; Turek *et al*. 1991; Sugano *et al*. 1992; Awaga *et al*. 1992*a*, 1994*a*, *b*; Hernàndez *et al*. 1993; Tamura *et al*. 1993; Panthou *et al*. 1993; Inoue & Iwamura 1993; Sugawara *et al*. 1994; Matsushita *et al*. 1997; Akita *et al*. 1995; Cirujeda *et al*. 1995; Okuno *et al*. 1995) since the discovery of the first pure organic ferromagnet, *p*-nitrophenyl nitronylnitroxide (Kinoshita *et al*. 1991). The nitronylnitroxides have also been known as a bidentate ligand for various transition and rare-earth metal ions. Ferromagnetic ground states have been observed in these complexes (Gatteschi *et al*. 1987; Caneschi *et al*. 1988, 1989; Benelli *et al*. 1993). Besides the ferromagnetic properties, it is notable that the solid-state nitronylnitroxides often exhibit unusual crystal structures.

The electronic structures of the nitronylnitroxides have been examined by means of electron paramagnetic resonance (Davis *et al*. 1972; Takui *et al*. 1995; D'Anna & Wharton 1970), ultraviolet photoelectron spectroscopy (Awaga *et al*. 1993), neutron diffraction (Ressouche *et al*. 1993; Zheludev *et al*. 1994) and NMR (Maruta *et al*. 1999). This radical family possesses a strong spin polarization effect, mainly because of the spatial closeness between the unpaired π electron and the non-bonding electrons (n–π exchange interaction). It is believed that the spin polarization effect stabilizes triplet charge transfer (CT) excited states, and the admixture of these states to the ground state results in a ferromagnetic intermolecular interaction (Awaga *et al*. 1987). This mechanism was originally proposed by McConnell (1967), and the theoretical importance of the spin polarization effect was pointed out by Yamaguchi *et al*. (1986).

While chemical modifications for the substituent at the α-carbon in nitronylnitroxide have been carried out extensively by many groups, we prepared the molecular compounds of pyridyl and *N*-alkylpyridinium nitronylnitroxides, combining them with various acids and anions. The principal aim of this project was to expand the

chemistry of nitronylnitroxide and to discover new organic ferromagnets and more unusual crystal structures and properties. Another aim of the *N*-alkylpyridinium nitronylnitroxide cation project was to control the intermolecular arrangement for ferromagnetic interaction. It is known that the oxygen atoms in the nitronylnitroxide moiety possess a large negative polarized charge (Awaga *et al*. 1989). Therefore, the intermolecular arrangement caused by an electrostatic interaction between the oxygen and the pyridinium ring is naturally to be expected, as shown in scheme 1. The singly occupied molecular orbital (SOMO) of nitronylnitroxide is localized on the two NO groups, making a node on the middle α-carbon, and has little population in the aromatic substituent, while the other frontier closed-shell orbitals (NLUMO, NHOMO, etc.) are distributed on both the nitronylnitroxide moiety and the substituent (Awaga *et al*. 1989). Therefore, the distance between the two SOMOs is so long in this geometry that the antiferromagnetic interaction would be suppressed. The contact between the NO group and the pyridinium ring means an intermolecular interaction between the SOMO in molecule **1** and the NHOMO, NLUMO, etc., in **2**. The latter orbitals are orthogonal to the SOMO in **2** because they belong to the same molecule. This situation can be compared with the 90° superexchange interaction that is well known to be ferromagnetic in the field of inorganic chemistry and physics (Anderson 1963). A ferromagnetic interaction is to be expected in the geometry depicted in scheme 1.

The molecular compounds of the pyridyl and pyridinium nitronylnitroxides prepared by our group are summarized in scheme 2. The *N*-protonation of pyridyl nitronylnitroxide was carried out by the reaction with HBr. The obtained materials were (pyridyl nitronylnitroxide)$_2$HBr in which the proton bridged two pyridyl ring with a $[NHN]^+$ hydrogen bond (Okuno *et al*. 1995). We also prepared various acid–base complexes of pyridyl nitronylnitroxide (Otsuka *et al*. 1998, 1997). The *N*-alkylpyridinium nitronylnitroxides were combined with various anions, such as, I^-, ClO_4^-, BF_4^-, MCl_4^{2-} (M = Mn^{2+} ($S = 5/2$) and Co^{2+} ($S = 3/2$)), $[Ni(dmit)_2]^-$, $[Mn_{12}O_{12}(O_2CPh)_{16}(H_2O)_4]^-$, etc. (Awaga *et al*. 1992*b*, 1994*a*; Yamaguchi *et al*. 1996; Imai *et al*. 1996; Takeda & Awaga 1997). Besides these works, a pyridinium nitronylnitroxide was used as a counter cation for a Cu^{2+}–Mn^{2+} bimetallic complex anion by Kahn and co-workers (Stump *et al*. 1993). In the course of our study, we obtained quite unusual spin systems: Kagome lattice and spin ladder, which are topics of the research on low-dimensional magnetic materials. In this paper we will describe the crystal structures and properties of the two systems found in the molecular compounds of nitronylnitroxide.

2. Organic Kagome antiferromagnets, *m*-MPYNN · X

Geometrical frustration in antiferromagnetic systems with triangular coordination symmetry is of interest to recent physics. In such a triangle, two nearest neighbours to a given spin are themselves nearest neighbours and antiferromagnetic couplings among them cannot be completely satisfied. The frustration prevents long-range magnetic order from being established and allows novel kinds of low-temperature magnetic states to develop (Fazekas & Anderson 1974; Wen *et al*. 1989; Chandra & Coleman 1991). The Heisenberg Kagome antiferromagnet, whose lattice is shown in scheme 3, is one of the most interesting of the frustrated systems (Syozi 1951). While the number of the nearest neighbours is six in the simple triangular lattice,

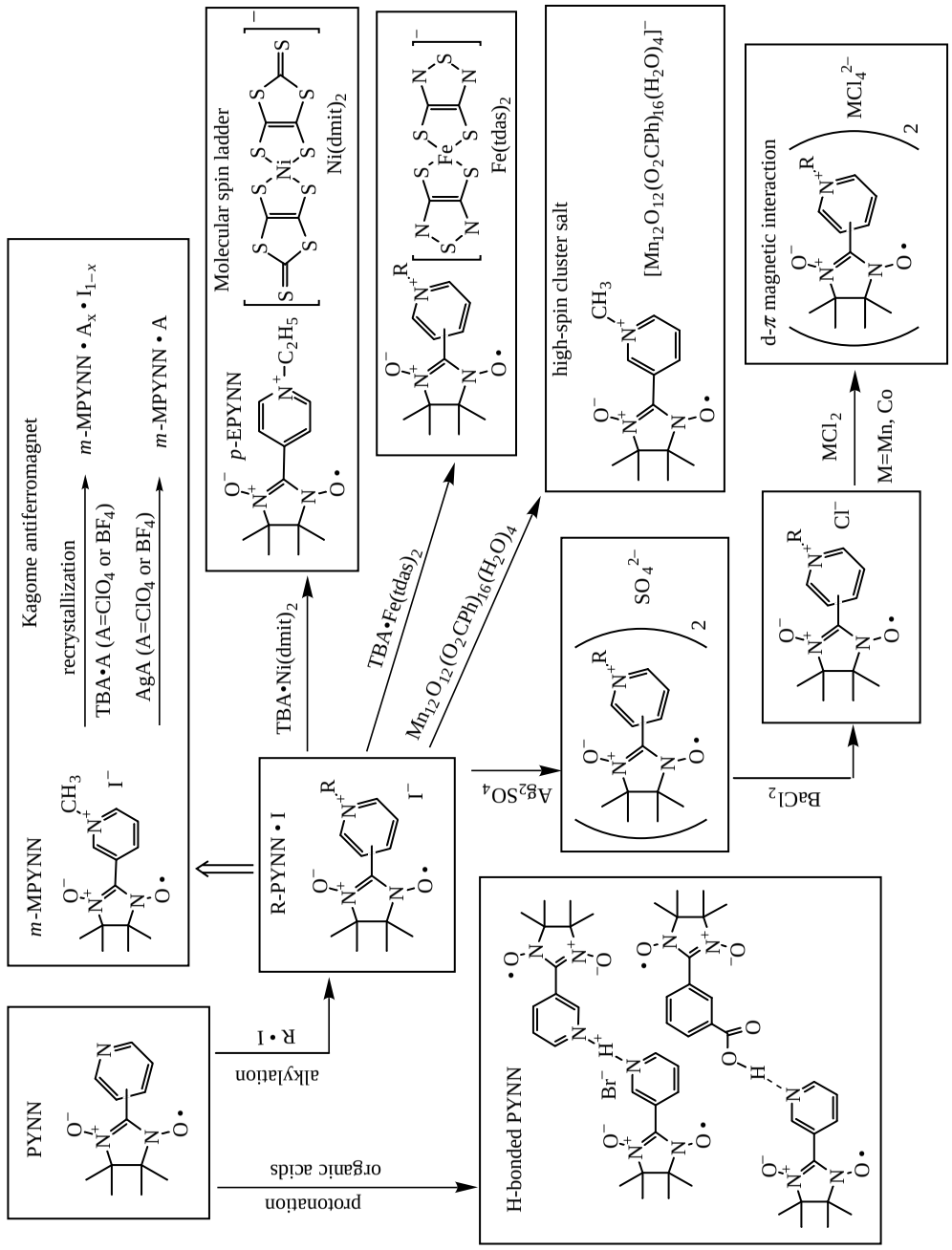

Scheme 2.

it is decreased to be four in the Kagome lattice. This fact permits more freedom for the alignment of the magnetic moments on the Kagome lattice, so that the Kagome antiferromagnets are predicted to exhibit rich non-trivial ground-state degeneracy. The actual ground state may be governed by subtle effects, such as a quantum

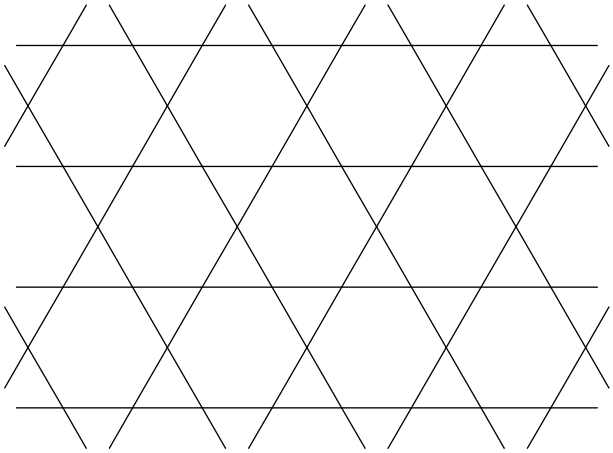

Scheme 3.

effect, a single-ion magnetic anisotropy, next-nearest-neighbour interactions, and so on.

From the viewpoint of materials, the spin-frustrated systems which have been experimentally studied so far are limited in inorganic materials (Ramirez 1991). Among them, the mineral hydronium jarosite (Wills & Harrison 1996) and the two-dimensional solid ^{3}He adsorbed on graphite (Estner *et al*. 1993; Siqueira *et al*. 1997) are known as Kagome magnets.

(*a*) *Unusual crystal structure of m*-MPYNN · X

Recently we found that the crystals of *m*-*N*-methylpyridinium nitronylnitroxide (abbreviated as *m*-MPYNN) involve an antiferromagnetic Kagome lattice (Awaga *et al*. 1992*b*, 1994*a*). As shown in scheme 2, *m*-MPYNN · I was obtained by the reaction of *m*-pyridyl nitronylnitroxide and methyl iodide. Recrystallization of *m*-MPYNN · I with the presence of excess TBA · A (TBA = tetrabutylammonium, and A = BF_4, ClO_4) gave a crystalline solid solution, *m*-MPYNN · A_x · I_{1-x}. The reaction of equivalent amounts of *m*-MPYNN · I and Ag · A resulted in immediate precipitation of Ag · I, leaving iodide-free *m*-MPYNN · A in the solution. Recrystallization of *m*-MPYNN · I, *m*-MPYNN · A_x · I_{1-x} and *m*-MPYNN · A from their acetone solutions resulted in hexagonal-shaped single crystals, including one acetone molecule per three *m*-MPYNN. The crystals of the simple iodide salt, *m*-MPYNN · I · ($\frac{1}{3}$)(acetone), were not stable: in the air they immediately turned into mosaic by evaporation of the crystal solvent, but the other crystals including BF_4^- or ClO_4^- were stable.

The structure of *m*-MPYNN · X · ($\frac{1}{3}$)(acetone) (X = I, BF_4, ClO_4, etc.) belongs to a trigonal space group. The *m*-MPYNN molecules exist as a dimer, and the dimer units form a two-dimensional triangular lattice parallel to the *ab*-plane. Figure 1*a* shows a projection of the organic layer of *m*-MPYNN onto the *ab*-plane. The radical dimer is located on each side of the triangles. In other words, the *m*-MPYNN molecules form a bond-alternated hexagonal lattice, as shown schematically in figure 1*b*. In the intradimer arrangement there is a very short intermolecular interatomic distance of less than 3 Å between the NO group and the pyridinium ring.

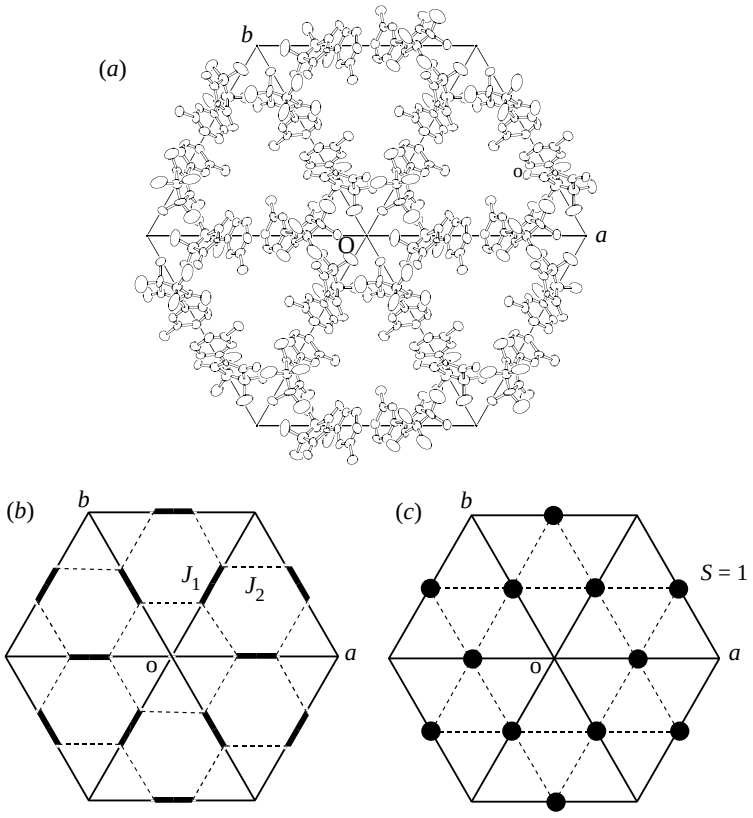

Figure 1. (*a*) Organic two-dimensional layer of *m*-MPYNN projected onto the *ab*-plane. (*b*) Bond-alternated hexagonal lattice. The parameters, J_1 and J_2, are intradimer and interdimer magnetic interactions, respectively. (*c*) Kagome lattice.

This short contact is probably caused by an electrostatic interaction between the positive charge on the pyridinium ring and the negative charge polarized on the O atom. As explained before, this is a wanted arrangement in which a ferromagnetic coupling can be expected. In the interdimer arrangement, on the other hand, there is a weak contact between the NO groups. The NO···NO contact means an overlap between SOMOs, which always contributes to antiferromagnetic coupling.

Figure 2 shows a side view of the trigonal lattice, where nine units of the *m*-MPYNN dimers on the surface of the hexagonal prism are drawn. The unit cell includes two organic layers at the heights of $z = 0$ and $z = \frac{1}{2}$, between which there is a large separation. A third of the anions are in the organic layer, joining the *m*-MPYNN molecules, and the remainder are between the layers, compensating the excess of positive charge in the organic layers. The crystal solvent, acetone, is located between the organic layers at the centre of the triangle.

(*b*) *Magnetic properties of* *m*-MPYNN · X

X-band EPR measurements were performed on the *m*-MPYNN·ClO_4·($\frac{1}{3}$)(acetone) single crystal (Awaga *et al*. 1994*a*; Hasegawa *et al*. 1995). The lineshape at room

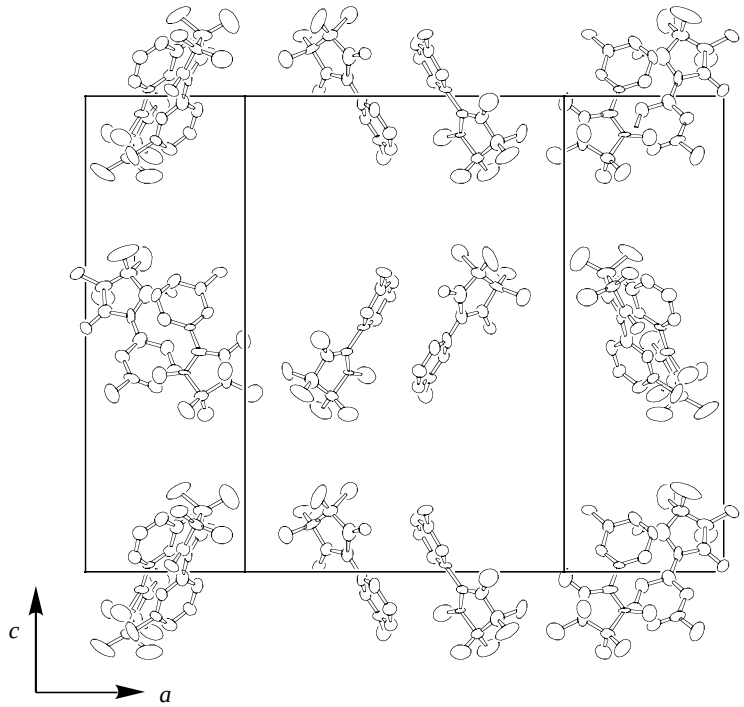

Figure 2. Side view of the organic two-dimensional layers. Nine *m*-MPYNN dimers on the surface of the hexagonal prism are drawn.

temperature was close to a Lorentzian shape, while it depended slightly on direction of the external field. Whereas one-dimensional magnetic systems exhibit EPR lines with large deviation from the Lorentzian, the deviation of a two-dimensional system is very small (Richards & Salamon 1974). From angular dependence experiments, the principal g values were obtained to be $g_{\parallel} = 2.0060$ and $g_{\perp} = 2.0058$, where $g_{\parallel}$ and $g_{\perp}$ are those values of g which are parallel and perpendicular to the c-axis, respectively. The g-value anisotropy in m-MPYNN$\cdot$ClO$_4\cdot(\frac{1}{3})$(acetone) was small, as well as those in most of the organic radicals. We examined the temperature dependence of $g_{\parallel}$ and $g_{\perp}$ and found a g-value shift below 100 K that depended seriously on the crystal shape. It was well explained in terms of the demagnetizing effect expressed by the Kittel's equation for the ferromagnetic resonance (Kittel 1947, 1948).

Figure 3 shows the angular dependence of the peak-to-peak linewidth ΔH_{pp} in the ac (open circles) and ab (closed circles) planes at room temperature. θ is the angle between the external field and the c-axis in the ac-plane and that between the field and the a-axis in the ab-plane, respectively. When the field is in the ab-plane the linewidth shows no dependence on the field direction, but when the field is in the ac-plane it makes minimums at the magic angles. The angular dependence can be well fitted to the theoretical equation (Richards & Salamon 1974)

$$\Delta H_{\mathrm{pp}} = A(3\cos^2\theta - 1)^2 + B, \tag{2.1}$$

where θ is the angle between the field and the c-axis. The solid curves in figure 3 show the best fits, obtained with $A = 0.094$ mT and $B = 0.259$ mT. Since the

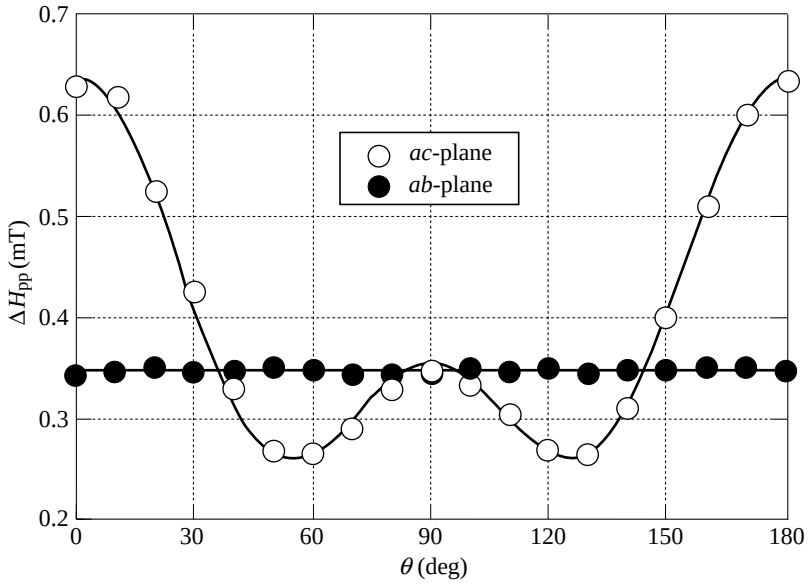

Figure 3. Angular dependence of the peak-to-peak linewidth of the m-MPYNN $\cdot$ $ClO_4 \cdot (\frac{1}{3})$(acetone) single crystal, in the ac (open circles) and ab (closed circles) planes. θ is the angle between the field and the c-axis in the ac-plane, and that between the field and the a-axis in the ab-plane, respectively.

EPR measurements concluded the two-dimensional Heisenberg-spin character, the magnetic properties of the material would be governed by the two parameters: the intradimer interaction J_1 and the interdimer interaction J_2, shown in figure 1*b*.

The temperature dependence of the paramagnetic susceptibilities χ_p for the m-MPYNN$\cdot BF_4 \cdot (\frac{1}{3})$(acetone) is shown in figure 4, where $\chi_p T$ is plotted as a function of temperature. The value of $\chi_p T$ increases as the temperature is decreased from room temperature down to *ca.* 10 K, indicating a ferromagnetic interaction. The intradimer ferromagnetic coupling J_1 is confirmed. After passing through a maximum near 10 K, $\chi_p T$ shows a quick decrease which suggests that the interdimer magnetic interaction J_2 is antiferromagnetic. The observed behaviour is quite consistent with the intradimer and the interdimer molecular arrangements. The observed temperature dependence can be interpreted well in terms of the ferromagnetic J_1 and the antiferromagnetic J_2, using

$$\chi = \frac{4C}{T\{3 + \exp(-2J_1/k_B T)\} - 4J_2/k_B T}, \tag{2.2}$$

where C is the Curie constant and k_B is the Boltzmann constant. The derivation of equation (2.2) is described elsewhere (Awaga *et al.* 1994*a*). The solid curve in figure 4 is the theoretical best fit to the data, obtained with $J_1/k_B = 11.6$ K and $J_2/k_B = -1.6$ K. Below $|J_1|/k_B$ K, the radical dimer can be regarded as a spin-1 Heisenberg spin which is located at the midpoint of each side of the triangle, as shown in figure 1*c*. It is expected that the interdimer antiferromagnetic coupling J_2 gives rise to spin frustration among the triplet spins. The spin lattice in figure 1*c* is exactly coincident with the Kagome lattice. Therefore, the magnetic system in this

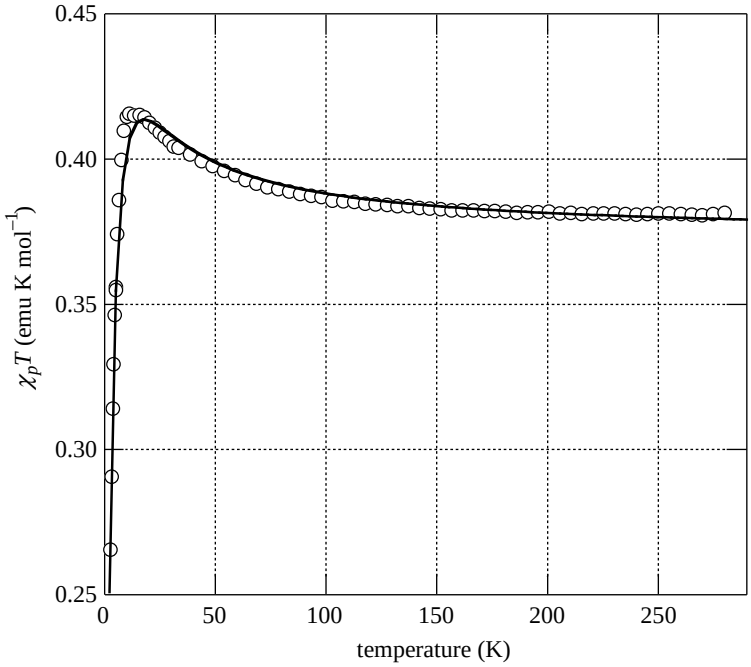

Figure 4. Temperature dependence of the paramagnetic susceptibilities χ_p for m-MPYNN $\cdot$ BF_4 $\cdot$ $(\frac{1}{3})$(acetone).

organic material will be characterized as a spin-1 Kagome antiferromagnet in the temperature range below $|J_2|/k_B$ K.

Figure 5 shows the temperature dependence of the AC magnetic susceptibilities χ_{AC} for the oriented single crystals of m-MPYNN $\cdot$ BF_4 $\cdot$ $(\frac{1}{3})$(acetone) below 0.8 K (Wada *et al*. 1997). The magnetic field was parallel to the c-axis. The value increases with decreasing temperature down to 0.24 K, and, after passing through a maximum, it approaches to zero at the absolute zero. We have confirmed no magnetic anisotropy in this behaviour. This clearly indicates that the ground state is not an antiferromagnetic ordered state but a spin gap state. In fact the low-temperature data can be well fitted to the gap equation

$$\chi = A\left(\frac{\Delta}{k_B T}\right)^f \exp\left(-\frac{\Delta}{k_B T}\right), \tag{2.3}$$

where A is a constant and Δ is the magnetic gap. The parameter f depends on the density of the excited states against the excitation energy, but is fixed to be unity in the analyses (Bulaevskii 1969). The solid curve in figure 5 is the theoretical one obtained with $A = 0.52$ and $\Delta/k_B = 0.25$ K. The spin gap states have been observed in the spin Peierls systems (Jacobs *et al*. 1976) and the Haldene gap systems (Haldene 1983), although these precedents were one-dimensional magnetic systems. To our knowledge, this is the first example of a spin gap state found in the two-dimensional magnetic materials. It is worth noting here that Anderson predicted the so-called resonating valence bond (RVB) state on a triangular antiferromagnetic

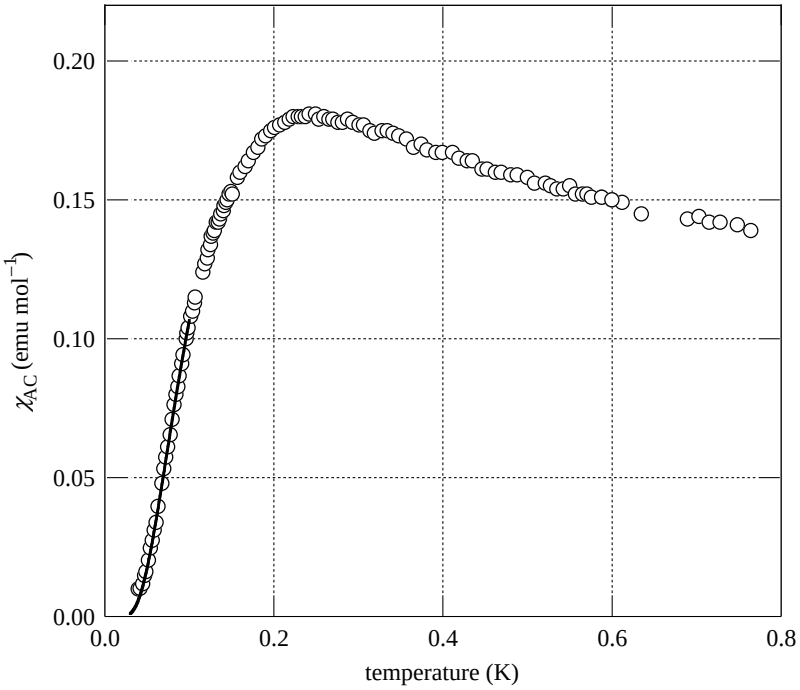

Figure 5. Temperature dependence of the AC magnetic susceptibilities χ_{AC} for the oriented single crystals of m-MPYNN $\cdot$ BF_4 $\cdot$ $(\frac{1}{3})$(acetone).

lattice, which also brought about a spin gap (Anderson 1973). It is possible that the ground state of the material can be characterized in terms of the RVB state.

(*c*) *Heat capacity of* m-MPYNN $\cdot$ X

The temperature dependence of the heat capacities c_p was examined down to 0.12 K on m-MPYNN $\cdot$ BF_4 $\cdot$ $(\frac{1}{3})$(acetone) (Wada *et al.* 1997). The results below 3 K are shown in figure 6. The value of c_p gradually increases with a decrease in temperature. After making a broad maximum at 1.4 K, c_p show a decrease. Below 0.24 K, where χ_{AC} shows the spin gap ground state, the value of c_p increases again. The temperature of the maximum c_p, namely 1.4 K, almost agrees with $|J_2|/k_B$. Monte Carlo calculation indicates that the heat capacity of the spin-1/2 Kagome Heisenberg antiferromagnet exhibits a maximum of short-range magnetic ordering at $1.4|J|/k_B$ (Nakamura & Miyashita 1995). The observed anomaly at 1.4 K is probably due to the short-range ordering made by J_2. The reason for the increase in c_p below 0.24 K is not clear, but it suggests another anomaly below 0.1 K. It is notable that there is no signal of long-range ordering in the temperature range down to 0.1 K, which corresponds to 8% of $|J_2|/k_B$. This supports the spin frustration in this magnetic system.

The plots of c_p/T show a gradual increase as the temperature is decreased down to 0.12 K (not shown). We calculated the entropy change accompanied with the anomaly at 1.4 K to be $\Delta S = 4.7\ \mathrm{J\,K^{-1}\,mol^{-1}}$, by using the data above 0.12 K and by subtracting the contributions of the lattice and the excited state due to

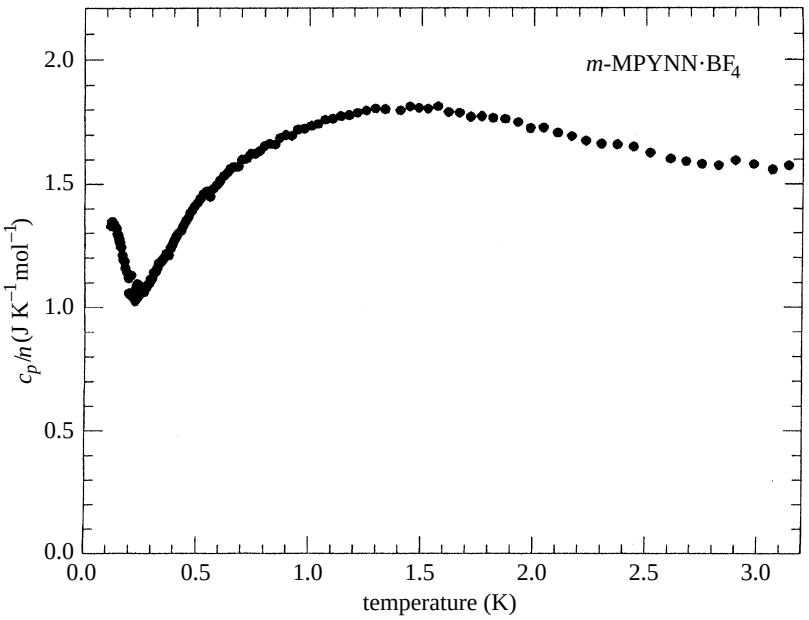

Figure 6. Temperature dependence of the heat capacities c_p for m-MPYNN $\cdot$ BF_4 $\cdot$ $(\frac{1}{3})$(acetone).

J_1. Since the triplet spins on the m-MPYNN dimers lose the magnetic freedom in the short-range ordering, the magnetic entropy is theoretically calculated to be $S_{\mathrm{m}} = (\frac{1}{2}R)\ln 3 = 4.567\,\mathrm{J\,K^{-1}\,mol^{-1}}$. The observed value of ΔS is already larger than S_{m}, despite the fact that ΔS was obtained using the data above 0.12 K. This means that there is an unknown degree of freedom besides the magnetic degree of freedom, which cooperates with the short-range magnetic ordering in this ultralow-temperature range.

(*d*) μ^+SR *of* m-MPYNN $\cdot$ X

We carried out muon spin relaxation on m-MPYNN $\cdot$ BF_4 $\cdot$ $(\frac{1}{3})$(acetone) in the temperature range down to 30 mK, to clarify whether magnetic transitions exist or not, and to confirm the non-magnetic ground state. Positive muon spin relaxation (μ^+SR) is a good microscopic probe to sense such a magnetic state of the system. A muon spin is completely polarized along a beam direction even in the zero-field (ZF) condition and depolarized after the stop at a potential-minimum position in the crystal of m-MPYNN $\cdot$ BF_4 interacting with a local field at a muon site (Uemura *et al*. 1985). A long-range or a short-range ordering of the dimer spins can be recognized as a change of the depolarization behaviour of the muon spin, because a static or a dynamically fluctuating component of the internal field which is accompanied by the magnetic transition affects strongly the muon spin polarization (Uemura *et al*. 1985; Mekata 1990).

Figure 7 shows ZF-μ^+SR time spectra obtained at 265 K, 100 K, 2.9 K and 30 mK. In this figure the asymmetry parameter of the muon spin at time t, $A(t)$, is defined as $[F(t) - B(t)]/[F(t) + B(t)]$, where $F(t)$ and $B(t)$ are muon events counted by the forward and backward counters, respectively. The asymmetry at each temperature

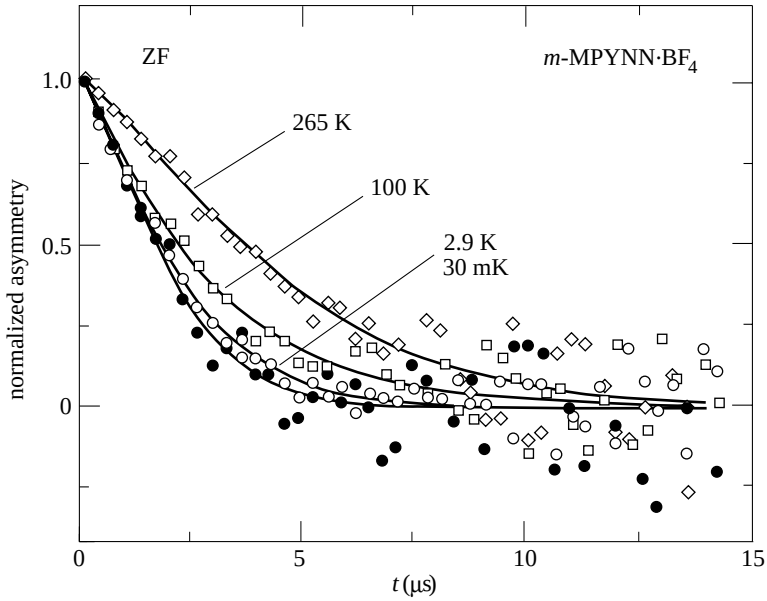

Figure 7. ZF-μ^+SR time spectra obtained for *m*-MPYNN $\cdot$ BF_4 $\cdot$ $(\frac{1}{3})$(acetone) at 265 K, 100 K, 2.9 K and 30 mK.

is normalized to be one at $t = 0$, to compare the difference of the depolarization behaviour. The depolarization behaviour cannot be described by either a simple Gaussian function or a Lorentzian function. For convenience sake, the obtained ZF-μ^+SR spectra were analysed by a power function, $A_0 \exp(-\lambda t)^\beta$, where A_0 is the initial asymmetry at $t = 0$ and λ is the depolarization rate. The solid curves in figure 7 are the best-fit results using this power function.

The temperature dependence of A_0, λ and β was obtained from the best-fit analysis. All parameters show the temperature independence below about 100 K, showing that static and dynamical properties of the local field at the muon site are temperature independent. This fact is different from other types of Kagome magnets in which strong enhancement of the depolarization rate by the critical slowing-down behaviour of magnetic moments is observed around a magnetic transition temperature (Keren *et al*. 1994, 1996; Uemura *et al*. 1994; Dunsiger *et al*. 1996). The parameter λ shows a slight decrease above 150 K, which is probably due to the motional narrowing effect indicating that the muon starts to diffuse through the crystal. From longitudinal-field dependence of the μ^+SR time spectra (not shown), a half-width of the distribution of the static internal field at the muon site ΔH was estimated to be 10 ± 2 G.

It is known that the muon implanted into a crystal which contains F^- ions forms the strong FμF state through a hydrogen bonding (Brewer *et al*. 1986). In this case, the distance between the F^- ion and the muon is similar to a nominal F^- ionic radius of 1.16 Å. Assuming that the distance between the stopped muon and the ^{19}F nucleus in *m*-MPYNN$\cdot BF_4$ is the nominal F^- ionic radius, the dipole field of the ^{19}F nucleus at the muon site is estimated to be about 8.5 G. This value is comparable to the obtained ΔH. Although the reason for the missing of the muon spin precession which has been observed in other fluorides (Brewer *et al*. 1986) is still unclear, it can be concluded that the implanted muon is expected to stop near the F^- ion forming

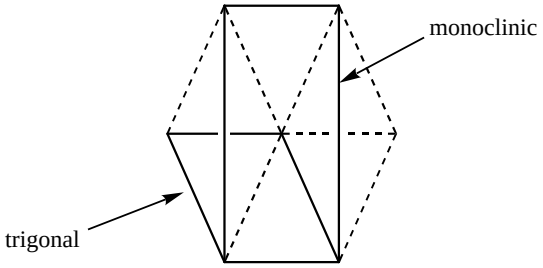

Scheme 4.

Table 1. *Cell and magnetic parameters for m-R-*PYNN · I

	m-MPYNN · I trigonal	*m*-EPYNN · I monoclinic	*m*-PPYNN · I monoclinic	*m*-BPYNN · I monoclinic
a (Å)	15.876(5)	16.14(6)	28.153(9)	9.794(2)
b (Å)		28.07(8)	16.407(14)	8.53(2)
c (Å)	23.583(6)	24.02(5)	24.705(11)	11.312(2)
β (deg)		91.1(2)	90.25(3)	104.19(2)
V (Å^3)	5147(3)	10 876(53)	11 411(11)	917(2)
Z	12	24	24	2
J_1/k_B	10.2	9.6	6.6	0.9
J_2/k_B	−1.6	−1.7	−1.0	−0.7

the hydrogen bonding and that the static internal field at the muon site originates from the ^{19}F nuclear dipole field.

In conclusion, the temperature independent depolarization behaviour which is due to the distributed static internal field induced by the ^{19}F nuclear dipoles at the muon site was observed down to 30 mK. The width of the field distribution was 10 ± 2 G. No clear long-range magnetic ordering of the dimer spins was observed. Taking into account the results of the magnetic susceptibility measurements, the ground state of *m*-MPYNN · BF_4 is concluded to be non-magnetic.

(*e*) *Magnetic properties of distorted Kagome lattices*

We have already studied the crystal structures and magnetic properties of the *para-R*-PYNN · I series, changing the length of the *N*-alkyl chain (Awaga *et al*. 1994*b*). Depending on the length, various crystal structures and magnetism were found. The chemical modification was a powerful tool to investigate the magnetostructural correlation in the crystals of the *R*-PYNN series. In this work, we prepared the iodide salts of the *meta-R*-PYNN series, where R = ethyl (E), *n*-propyl (P) and *n*-butyl (B), and compared their crystal structures and magnetic properties with those of *m*-MPYNN · I.

The materials were obtained by the same procedure as for *m*-MPYNN · I. The recrystallizations of *m*-EPYNN · I and *m*-PPYNN · I from their acetone or acetone/benzene solutions resulted in hexagonal-shaped single crystals, while *m*-BPYNN · I gave the block-shape single crystals. The elemental analyses indicated the following chemical formulae: *m*-EPYNN · I · 1.5H_2O, *m*-PPYNN · I · 0.5H_2O and

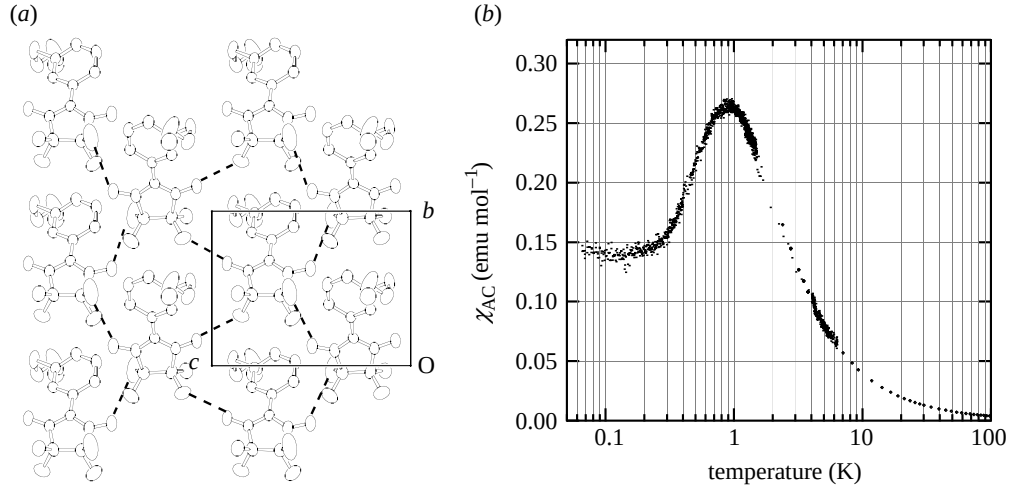

Figure 8. (*a*) A projection of the structure of *p*-BPYNN · I along the monoclinic *a*-axis. (*b*) Temperature dependence of the AC magnetic susceptibilities χ_{AC} for the *m*-BPYNN · I.

m-BPYNN · I. Table 1 shows the unit cell dimensions of the *m*-*R*-PYNN · I series, determined using X-ray diffraction data in the range $20° < 2\theta < 25°$. While the crystal of *m*-MPYNN · I belongs to the trigonal system, *m*-EPYNN · I, *m*-PPYNN · I and *m*-BPYNN · I crystallize into the monoclinic systems. However, it was found that lattice transformations for *m*-EPYNN · I and *m*-PPYNN · I lead to cell dimensions which were quite similar to those of *m*-MPYNN · I. Schematic comparison between the trigonal and monoclinic cells is shown in scheme 4. The transformed lattice constants are $a = 16.14(6)$ Å, $b = 16.19(4)$ Å, $c = 24.02(6)$ Å, $\alpha = 89.5(2)°$, $\beta = 90.1(2)°$, $\gamma = 119.9(1)°$, $V = 5440(53)$ Å^3 for *m*-EPYNN · I and $a = 16.30(1)$ Å, $b = 16.30(1)$ Å, $c = 24.71(1)$ Å, $\alpha = 89.7(4)°$, $\beta = 90.1(4)°$, $\gamma = 119.5(3)°$, $V = 5709(5)$ Å^3 for *m*-PPYNN · I. The obtained lattice parameters, *a*, *b* and *c*, and *V*, are slightly larger than the corresponding ones of *m*-MPYNN · I, but the differences between them are very small. Although we could not finish full structural analyses for *m*-EPYNN · I and *m*-PPYNN · I, probably because of positional disorders of the iodide ion and the crystal solvent, it is expected that they have a slightly distorted Kagome lattice. The decrease in crystal symmetry means distortion of the equilateral triangle to an isosceles triangle. This will significantly affect the low-temperature magnetic properties, as described later.

m-BPYNN · I crystallizes into a completely different structure. Figure 8*a* shows a projection of the structure along the monoclinic *a*-axis. The *m*-BPYNN molecules form a two-dimensional network caused by the contacts between the NO group and the methyl group in the nitronylnitroxide moiety. The hydrogen atoms in the methyl group, namely β-H atoms, have negative spin densities. It is believed that such contacts between the NO group and β-H atoms brings about a ferromagnetic interaction (Togashi *et al*. 1996).

Figure 9 shows the temperature dependence of $\chi_p T$ for the *m*-*R*-PYNN · I series. The plots for *m*-MPYNN · I, *m*-EPYNN · I and *m*-PPYNN · I show quite similar temperature dependence: the value of $\chi_p T$ increases, as temperature is decreased from room temperature down to *ca.* 10 K. After passing through a maximum, $\chi_p T$

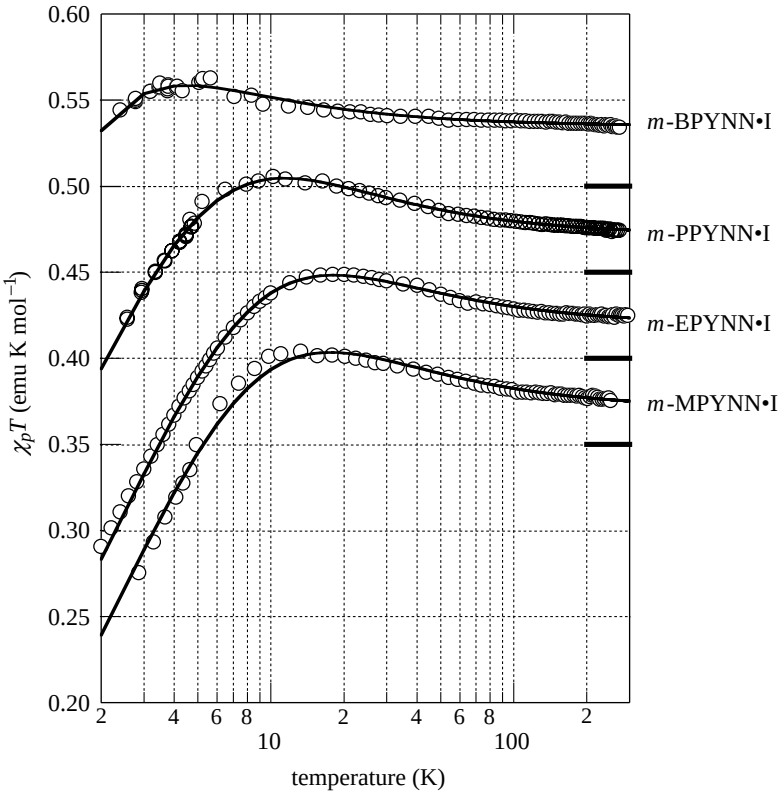

Figure 9. Temperature dependence of the paramagnetic susceptibilities χ_p for the *m*-*R*-PYNN · I series.

shows a quick decrease. Their temperature dependences are well explained by equation (2.1). Exactly speaking, *m*-EPYNN · I and *m*-PPYNN · I include two kinds of J_2, because of the distortion of the Kagome lattice in them. However, the distortion is so small that we ignore the difference. The solid curves going through the plots for *m*-MPYNN · I, *m*-EPYNN · I and *m*-PPYNN · I in figure 9 are the theoretical best fits to the data, obtained with the parameters listed in table 1. The values of J_1 and J_2 systematically decrease with the extension of the *N*-alkyl chain. Presumably this is caused by the expansion of the two-dimensional lattice.

The value of $\chi_p T$ for *m*-BPYNN · I shows a slight increase with a decrease in temperature down to *ca.* 5 K, and it decreases after passing through a maximum. This behaviour indicates coexistence of a stronger ferromagnetic interaction and a weaker antiferromagnetic coupling between the ferromagnetic units, but their intensities seem smaller than those in the other three salts. The crystal of *m*-BPYNN · I consists of the two-dimensional network shown in figure 8*a*. Assuming a ferromagnetic intralayer interaction J_1 and an antiferromagnetic interlayer interaction J_2, the temperature dependence was fitted to the equation

$$\chi = \frac{\chi'}{1 - \dfrac{2zJ_2}{N_{\mathrm{A}} g \mu_{\mathrm{B}}} \chi'} \tag{2.4}$$

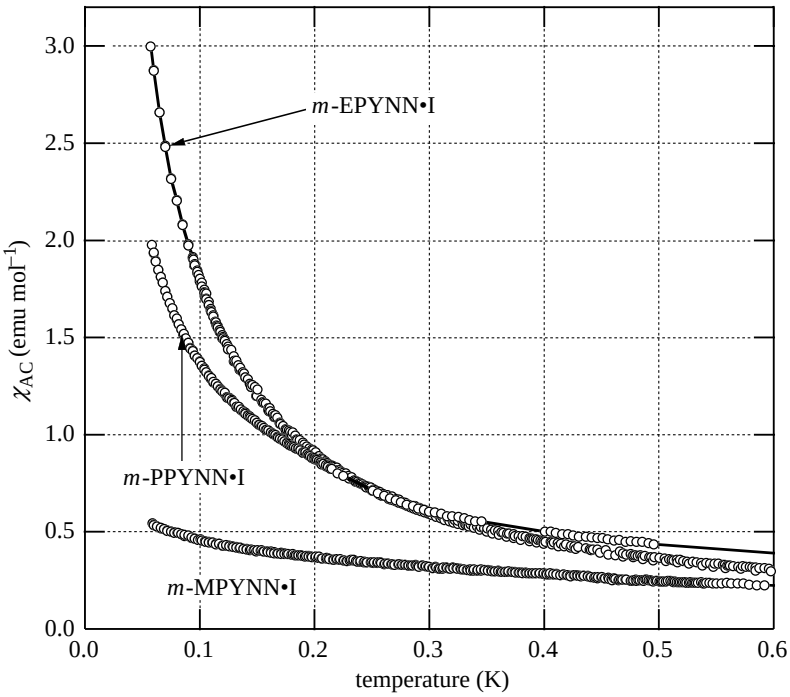

Figure 10. Temperature dependence of the AC susceptibilities χ_{AC} for m-MPYNN · I, m-EPYNN · I and m-PPYNN · I.

with

$$\chi' = \frac{C}{T}(1 + 2K + 2K^2 + \tfrac{4}{3}K^3 + \tfrac{13}{12}K^4) \quad \text{and} \quad K = \frac{J_1}{k_B T},$$

where z is the number of neighbouring layers and is equal to 2 in this case. The theoretical best fit was obtained with the parameters listed in table 1.

The temperature dependence of the AC susceptibilities χ_{AC} for m-MPYNN · I, m-EPYNN · I and m-PPYNN · I is shown in figure 10. Although m-MPYNN · I includes the regular antiferromagnetic Kagome lattice, as well as m-MPYNN · BF_4, the value of χ_{AC} continues to increase down to 0.05 K without showing the spin gap state. Probably this is caused by the fact that the salt is unstable because of evaporation of the crystal solvent. In fact the dependence can be explained by the equation

$$\chi = A\left(\frac{\Delta}{k_B T}\right)^f \exp\left(-\frac{\Delta}{k_B T}\right) + \frac{C_{def}}{T}, \tag{2.5}$$

where the first term is the same as equation (2.2) and the second term is for the Curie contribution of lattice defects. Fitting the data to equation (2.5), the parameters are obtained as follows: $A = 0.64$, $\Delta/k_B = 0.25$ K and $C_{def} = 0.025$ emu K mol^{-1} (6.6%). The values of A and Δ are very close to the corresponding parameters for m-MPYNN · BF_4. The distorted Kagome materials, m-EPYNN · I and m-PPYNN · I, show a similar temperature dependence, but their values of χ_{AC} below 0.2 K are approximately five times larger than that of m-MPYNN · I. It seems hard to attribute them to the contribution of lattice defects. It is considered that their behaviour is

intrinsic and the spin gap state is easily collapsed by the small distortion of the Kagome lattice.

The temperature dependence of χ_{AC} for *m*-BPYNN · I is shown in figure 8*b*. The value increases with decreasing temperature down to 0.9 K and, after passing through a maximum, it becomes nearly two-thirds of the maximum value at the lowest temperature. The heat capacity makes a maximum at 0.56 K (not shown). The magnetic and thermal behaviour strongly indicate an antiferromagnetic transition at 0.56 K. The antiferromagnetic transition is rationalized, because of the intralayer ferromagnetic interaction and the interlayer antiferromagnetic interaction. It is interesting that the *m*-BPYNN · I exhibits the highest transition temperature in the series, in spite of the fact that the magnetic interactions in it are weaker than those in the other three salts. This suggests that the magnetic properties of the Kagome and Kagome-like materials are governed by spin-frustration and that the frustration on the Kagome lattice prevents usual antiferromagnetic ordering.

(*f*) *Summary*

The crystal structures and magnetic properties of the *m*-*R*-PYNN · X series were studied. In the crystal of *m*-MPYNN · X, the ferromagnetic dimers formed the triangular lattice with the weak interdimer antiferromagnetic coupling. The magnetic system can be regarded as a spin-1 Kagome antiferromagnet at low temperatures. The single-crystal EPR concluded the two-dimensional Heisenberg character of the spin system. The low-temperature magnetic behaviour indicated the spin-gap ground state, which was possibly identical with the RVB state. The temperature dependence of the heat capacity showed the short-range magnetic ordering caused by the interdimer antiferromagnetic interaction, but did no long-range ordering down to 0.1 K. In addition, it suggested an unknown degree of freedom which cooperated with the short-range magnetic ordering. The μ^+SR exhibited the temperature-independent depolarization behaviour down to 30 mK. In other words, this study strongly supports no long-range magnetic ordering of the dimer spins and the non-magnetic ground state. With an extension of the *N*-alkyl chain in the *m*-*R*-PYNN · I series, distortion of the Kagome lattice took place, which resulted in collapse of the spin-gap ground state.

3. Molecular spin ladder, *p*-EPYNN · [Ni(dmit)$_2$]

There is an increasing interest in preparation of molecule-based materials which show multifunctional properties (Day 1993). One of the promising routes to the multifunctional materials is to synthesize molecular complexes consisting of two components with different physical properties. *N*-alkylpyridinium nitronylnitroxides are useful as a component of ferromagnetic property because they often exhibit ferromagnetic intermolecular interactions (Awaga *et al*. 1994*b*, 1992*b*). Nickel bis(4,5-dithiolato-1,3-dithiole-2-thione), abbreviated as [Ni(dmit)$_2$], is an electron acceptor molecule. The centric Ni ion can take three kinds of valence states: +2, +3 and +4, and the molecule shows corresponding oxidation states, namely [Ni(dmit)$_2$]$^{2-}$, [Ni(dmit)$_2$]$^-$ and [Ni(dmit)$_2$]^0, respectively. In particular, the mixed-valence state between [Ni(dmit)$_2$]$^-$ and [Ni(dmit)$_2$]^0, which can be achieved by an electrochemical method, attracts much interest because it often shows metallic conductivity and

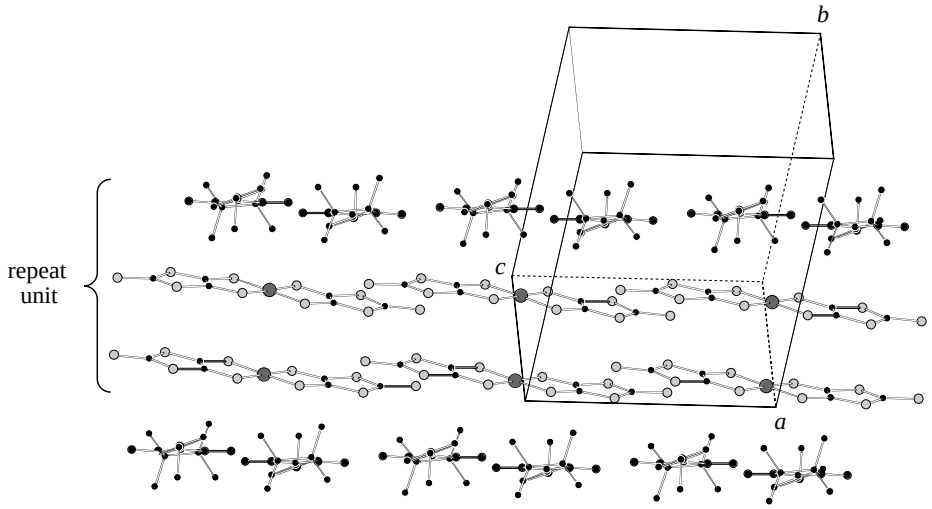

Figure 11. View of the crystal structure of p-EPYNN · [Ni(dmit)$_2$].

superconductivity (Brossard *et al*. 1986, 1988, 1989; Kobayashi *et al*. 1987, 1991, 1992; Tajima *et al*. 1993).

In this work, we studied the complexes of N-alkylpyridinium nitronylnitroxide cations and [M(dmit)$_2$] (M = Ni and Au) anions. While the aim of this research was to combine the magnetic property of nitronylnitroxide and the conductive property of [M(dmit)$_2$] and to obtain multifunctional molecule-based materials, we found a ladder structure of [Ni(dmit)$_2$] in the crystal of p-EPYNN · [Ni(dmit)$_2$], where p-EPYNN is p-N-ethylpyridinium nitronylnitroxide. After comparing the structures and magnetic properties of p-EPYNN · [Ni(dmit)$_2$] and p-EPYNN · [Au(dmit)$_2$], we will report the impurity effects on the molecular spin ladder.

(*a*) *Crystal structure and magnetic properties of* p-EPYNN · [Ni(dmit)$_2$]

The molecular complex, p-EPYNN·[Ni(dmit)$_2$], was obtained by a double-decomposition reaction between p-EPYNN · I and TBA · [Ni(dmit)$_2$] (Imai *et al*. 1996). Figure 11 shows a view of the crystal structure. Figure 12*a* represents the structure of p-EPYNN, in which slightly non-planar p-EPYNN cation radicals form an alternating chain along the c-axis with a side-by-side head-to-head arrangement. This chain is formed by short contacts between the nitronylnitroxide oxygen atom and the pyridinium ring, which are probably due to an electrostatic interaction. As explained in the previous section, a ferromagnetic coupling can be expected in the structure. Figure 12*b* shows the structure of [Ni(dmit)$_2$], in which [Ni(dmit)$_2$] exists as a face-to-face dimer. Further, the dimers are stacked along the c-axis with a translational relation, forming a ladder structure. There are unusually short S···S contacts in the interdimer arrangement. Since each [Ni(dmit)$_2$] is a doublet spin species, this structure can be regarded as a two-leg spin ladder. To our knowledge, this is the first example of a spin ladder found in a molecule-based material. As shown in figure 11, there is an alternation of the chain of p-EPYNN and the ladder of [Ni(dmit)$_2$] along the b-axis. In the arrangement between p-EPYNN and [Ni(dmit)$_2$], one [Ni(dmit)$_2$] molecule interacts with two pyridinium rings of p-EPYNN. Since the unpaired elec-

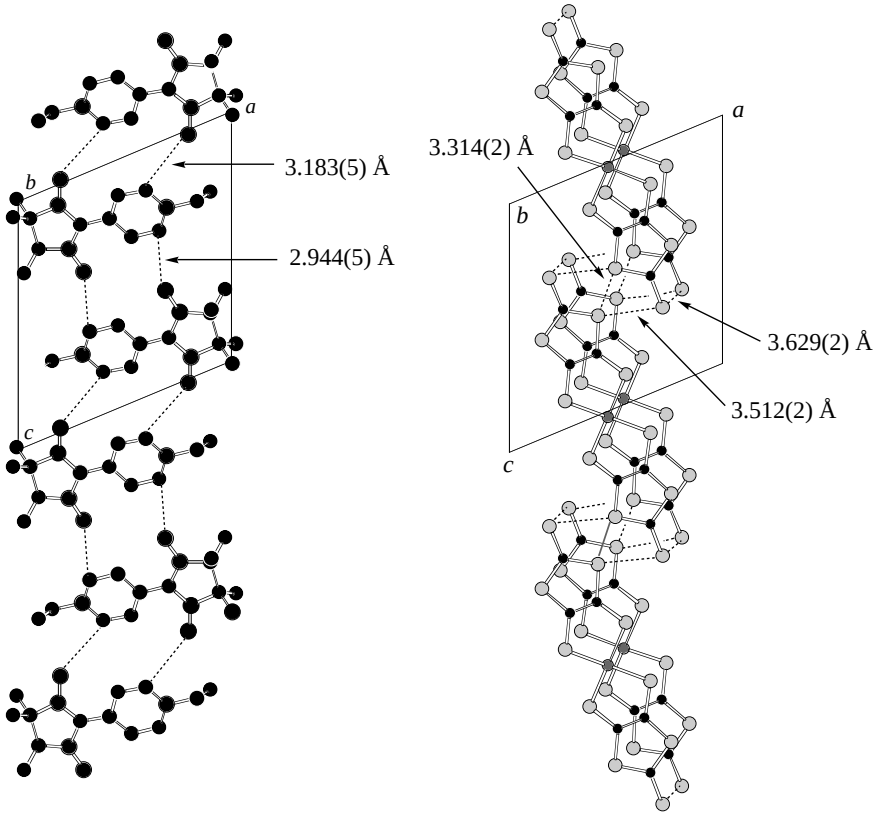

Figure 12. Projections of the structures of (*a*) *p*-EPYNN and (*b*) $[Ni(dmit)_2]$ in *p*-EPYNN · $[Ni(dmit)_2]$ along the *b*-axis.

tron is localized on the NO groups in the nitronylnitroxide, the magnetic interaction between the cation and the anion seems weak.

The temperature dependence of $\chi_p T$ for *p*-EPYNN · $[Ni(dmit)_2]$ is depicted in figure 13 (Imai *et al*. 1996). With an increase in temperature from 2 K, the value of $\chi_p T$ quickly decreases and, after passing through a plateau in the temperature range 40–150 K, it gradually increases. This behaviour can be well understood by taking into account two contributions: the dark grey part is from the chain of *p*-EPYNN, which shows a weak ferromagnetic property; the light grey part is from $[Ni(dmit)_2]$, which exhibits an activation-type susceptibility. The susceptibility data are analysed using the following equation:

$$\chi(T) = \frac{2C_1}{\sqrt{\pi(a/k_B)T}} e^{-\Delta/k_B T} + \frac{C_2}{T}\left(\frac{1 + A_1K + A_2K^2 + A_3K^3 + A_4K^4 + A_5K^5}{1 + A_6K + A_7K^2 + A_8K^3}\right)^{2/3}, \tag{3.1}$$

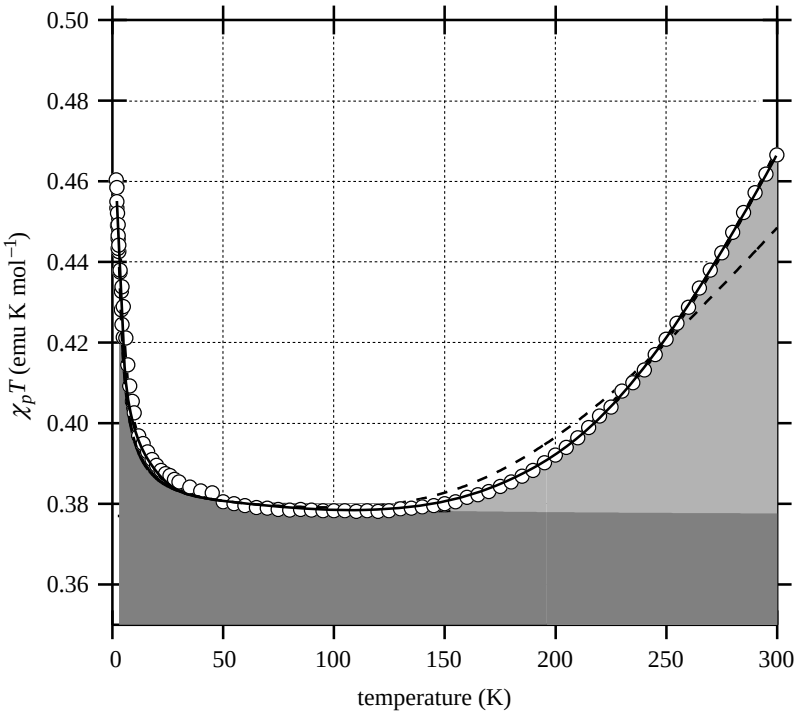

Figure 13. Temperature dependence of the paramagnetic susceptibilities χ_p for p-EPYNN · [Ni(dmit)$_2$].

with

$$K = \frac{J_{\mathrm{F}}}{k_{\mathrm{B}}T},$$

where the first term expresses the contribution of the spin ladder chain and the second term expresses the contribution of the one-dimensional ferromagnetic chain. The parameter Δ is the magnetic gap, $a = \frac{1}{2}[\partial^2\varepsilon(k)/\partial k^2]_{k=\pi}$, where $\varepsilon(k)$ is the energy dispersion of the spin wave excitation in the spin ladder of [Ni(dmit)$_2$], J_{F} is the ferromagnetic exchange coupling constant of p-EPYNN, and C_1 and C_2 correspond to the Curie constants for [Ni(dmit)$_2$] and p-EPYNN, respectively. The parameters A_1–A_9 are defined in Baker *et al.* (1964). The first term deriving from the gap equation, namely equation (2.2), was obtained to fit the magnetic susceptibility of the spin ladders (Troyer *et al.* 1994). The solid curve in figure 13 represents the best fit to the experimental data obtained with $\Delta/k_{\mathrm{B}} = 940$ K, $a/k_{\mathrm{B}} = 13.6$ K and $J_{\mathrm{F}}/k_{\mathrm{B}} = 0.32$ K. The parameters C_1 and C_2 are fixed to be 0.375 emu K mol^{-1} ($g = 2.00$) and 0.394 emu K mol^{-1} ($g = 2.05$), respectively. The broken curve in this figure is the theoretical trial fit of the dimer model with $\Delta/k_{\mathrm{B}} = 870$ K, which indicates significant deviation from the experimental plots.

Quantum spin ladders, which fill the gap between one- and two-dimensional quantum magnets, are attracting much interest. It is well known that one-dimensional antiferromagnetic chains of Heisenberg doublet spins exhibit a non-zero magnetic susceptibility at absolute zero. Their ground states are non-magnetic, but the excitation of a paramagnetic spin wave from the ground state costs no energy. This

gap-less structure in energy results in the non-zero susceptibility. Recently, theorists have found that the crossover between the dimensions is not at all smooth, depending on whether the number of legs in the ladder is even or odd (Rice *et al*. 1994). They found a spin gap for the even-leg spin ladders, because of formation of the RVB states. The presence of spin gap in the two-leg spin ladders was already proved in several inorganic materials (Johnston *et al*. 1987; Azuma *et al*. 1994), and the above analysis for the molecular spin ladder also concluded the spin gap: the intrinsic χ_p for [Ni(dmit)$_2$] became zero at low temperatures.

We also carried out conductivity measurements on *p*-EPYNN · [Ni(dmit)$_2$]. The material was an anisotropic semiconductor whose conductivity along the *c*-axis, namely, the ladder direction, was about 10^{-4} S cm^{-1} and the activation energy was 0.27 eV. The important point was that the conductivity perpendicular to the *c*-axis was worse than this by three orders of magnitude.

To our knowledge, there have been two reports on new molecular spin ladders since we found *p*-EPYNN · [Ni(dmit)$_2$] (Rovira *et al*. 1997; Komatsu *et al*. 1997). It is highly possible that the molecular spin ladders will add valuable contributions to the studies of the spin ladders, the RVB states, etc.

(*b*) *Crystal structure and magnetic properties of* *p*-EPYNN · [Au(dmit)$_2$]

The complex *p*-EPYNN · [Au(dmit)$_2$] was prepared by the same procedure as for *p*-EPYNN · [Ni(dmit)$_2$]. *p*-EPYNN · [Au(dmit)$_2$] crystallizes into a structure that is different form that of *p*-EPYNN[Ni(dmit)$_2$], but there are interesting similarities between the two structures. Figure 14*a* shows the structure of *p*-EPYNN in *p*-EPYNN · [Au(dmit)$_2$], projected along the *b*-axis. There is a one-dimensional chain of *p*-EPYNN along the *c*-axis in which the molecules are arranged head-to-tail and side-by-side. This pattern is very similar to that in the crystal of *p*-EPYNN · [Ni(dmit)$_2$]. Figure 14*b* shows the structure of [Au(dmit)$_2$] projected along the *b*-axis. The [Au(dmit)$_2$] anions make two independent stacking chains, A and B, along the *c*-axis with short S···S contacts. However, there is no face-to-face overlapping between the [Au(dmit)$_2$] chains, in contrast to the [Ni(dmit)$_2$] anions which exhibit the face-to-face dimers in *p*-EPYNN · [Ni(dmit)$_2$]. This is probably caused by the fact that the diamagnetic [Au(dmit)$_2$] cannot gain exchange energy by dimerization. Along the *a*-axis there is an alternation of the *p*-EPYNN chain and the chain A of [Au(dmit)$_2$], in which the cation–anion arrangement is very similar to that in *p*-EPYNN · [Ni(dmit)$_2$].

The temperature dependence of $\chi_p T$ for *p*-EPYNN · [Au(dmit)$_2$] is shown in figure 15. The value is almost constant at high temperatures, and shows an increase below 50 K. The behaviour can be interpreted in terms of the ferromagnetic chain, using

$$\chi = \frac{C}{T}\left(\frac{1 + A_K + A_2K^2 + A_3K^3 + A_4K^4 + A_5K^5}{1 + A_6K + A_7K^2 + A_8K^3}\right)^{2/3}, \tag{3.2}$$

with

$$K = \frac{J_{\mathrm{F}}}{k_{\mathrm{B}}T}.$$

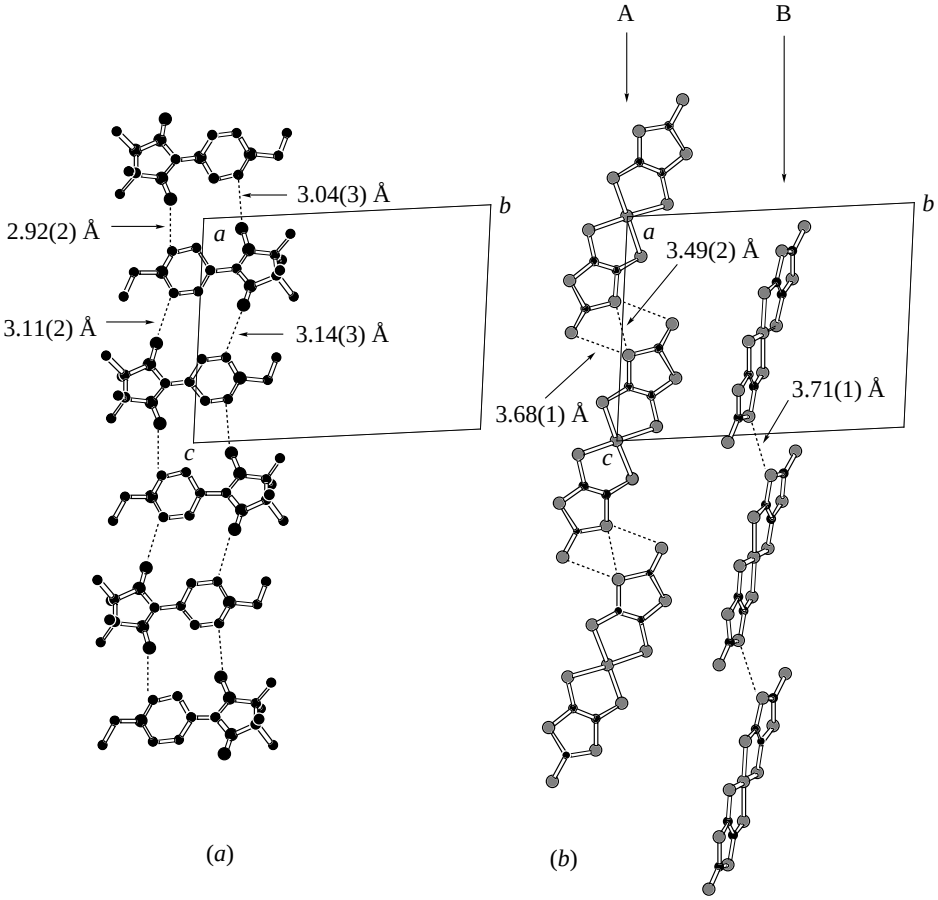

Figure 14. Projections of the structures of (*a*) *p*-EPYNN and (*b*) $[Au(dmit)_2]$ in *p*-EPYNN $\cdot$ $[Au(dmit)_2]$ along the *b*-axis.

The best fit, depicted as a solid curve in figure 15, is obtained with the parameters $C = 0.375\,\text{emu K mol}^{-1}$ (fixed) and $J_F/k_B = 0.38\,\text{K}$. This justifies the analysis of the magnetic data of *p*-EPYNN $\cdot$ $[Ni(dmit)_2]$ shown in figure 13.

(*c*) *Magnetic properties of* *p*-EPYNN $\cdot$ $[Ni(dmit)_2]_{1-x} \cdot [Au(dmit)_2]_x$

In the crystal of *p*-EPYNN $\cdot$ $[Ni(dmit)_2]$, the $[Ni(dmit)_2]$ anions form the spin ladder with the spin gap of 940 K, sandwiched by the ferromagnetic chains of *p*-EPYNN. In the crystal of *p*-EPYNN$\cdot$$[Au(dmit)_2]$, *p*-EPYNN forms the ferromagnetic chain which is very similar to that in *p*-EPYNN $\cdot$ $[Ni(dmit)_2]$ and $[Au(dmit)_2]$ forms the two independent chains. It is known that the monovalent anions, $[Ni(dmit)_2]^-$ and $[Au(dmit)_2]^-$, make a solid solution in the salt of n-Bu_4N^+ (Kirmse *et al.* 1980). In this work we prepared a solid solution system, *p*-EPYNN $\cdot$ $[Ni(dmit)_2]_{1-x} \cdot [Au(dmit)_2]_x$, in order to elucidate impurity effects on the magnetic properties of the molecular spin ladder.

The solid solutions were obtained by the reaction of the three components: *p*-EPYNN $\cdot$ I, TBA $\cdot$ $[Ni(dmit)_2]$ and TBA $\cdot$ $[Au(dmit)_2]$. The cell parameters for the

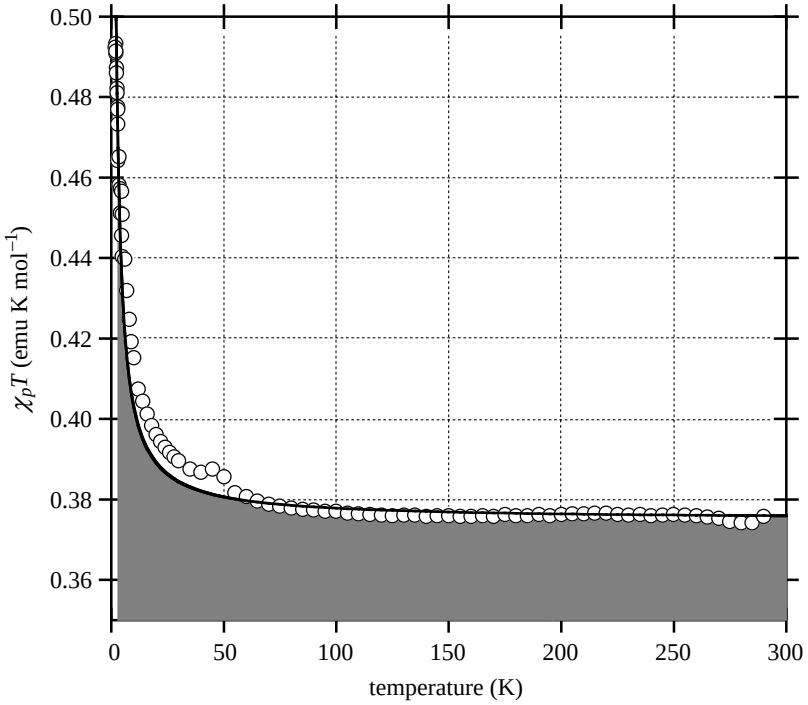

Figure 15. Temperature dependence of the paramagnetic susceptibilities χ_p for p-EPYNN $\cdot$ [Au(dmit)$_2$].

Table 2. *Cell parameters for* p-EPYNN $\cdot$ [Ni(dmit)$_2$]$_{1-x}$ $\cdot$ [Au(dmit)$_2$]$_x$

	$x = 0.0$ triclinic	$x = 0.5$ triclinic	$x = 1.0$ triclinic
a (Å)	11.647(4)	11.704(6)	14.399(4)
b (Å)	11.986(3)	12.062(9)	16.524(4)
c (Å)	12.047(6)	12.091(5)	12.743(3)
α (deg)	103.25(3)	102.92(6)	92.71(2)
β (deg)	106.01(3)	106.07(5)	100.08(2)
γ (deg)	109.91(2)	110.49(4)	103.65(2)
V (Å^3)	1419.4(9)	1435(2)	2888(1)
Z	2	2	4

three crystals, p-EPYNN $\cdot$ [Ni(dmit)$_2$]$_{1-x}$ $\cdot$ [Au(dmit)$_2$]$_x$ of $x = 0.0$, 0.5 and 1.0, are compared in table 2. It is found that the $x = 0.5$ crystal is isomorphous to the $x = 0$ crystal, namely p-EPYNN $\cdot$ [Ni(dmit)$_2$], which involves the spin ladder. It is reasonable to assume that the solid solutions of $0 \leqslant x \leqslant 0.5$ are all isomorphous to p-EPYNN $\cdot$ [Ni(dmit)$_2$].

The temperature dependence of the magnetic susceptibilities for the solid solutions of $x = 0$, 0.1, 0.25 and 0.5 were examined. The results are shown in figure 16, where the product $\chi_p T$ is plotted as a function of temperature. The closed circles

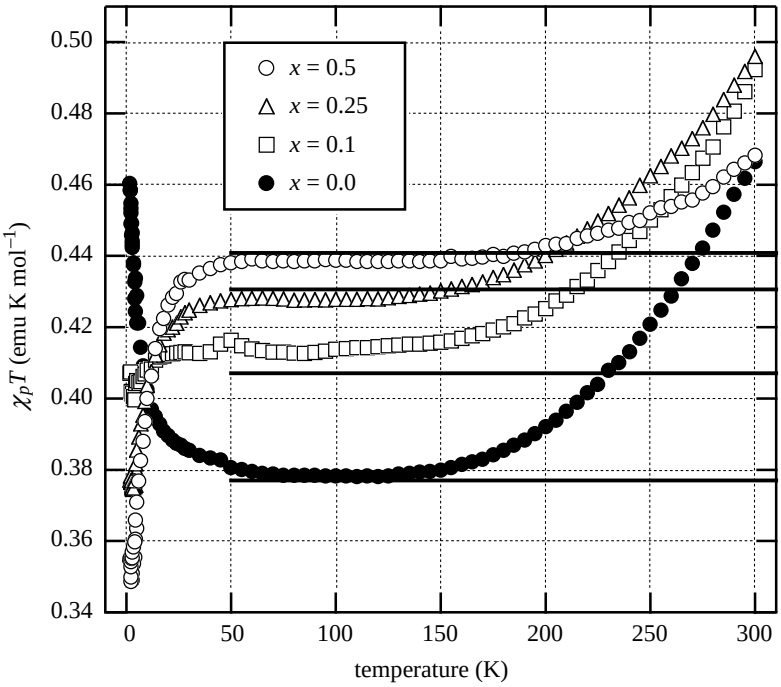

Figure 16. Temperature dependence of the paramagnetic susceptibilities χ_p for p-EPYNN $\cdot$ [Ni(dmit)$_2$]$_{1-x}$ $\cdot$ [Au(dmit)$_2$]$_x$ of $x = 0$, 0.1, 0.25 and 0.5.

show the results on p-EPYNN $\cdot$ [Ni(dmit)$_2$], which were already explained in the previous section. As the value of x is increased, the $\chi_p T$ value at the plateau shows a significant increase. Probably this is caused by an increase of the paramagnetic [Ni(dmit)$_2$] anions which pair with the doped [Au(dmit)$_2$] in the ladder. Assuming that such paramagnetic lattice defects were randomly distributed in the ladder and followed the Curie law, the $\chi_p T$ values at the plateaus for the four crystals were calculated. The solid lines in figure 16 show the theoretical values. They can explain the rise of the plateaus quantitatively. The probable Curie behaviour of [Ni(dmit)$_2$] on the defects indicates that the exchange coupling constant perpendicular to the ladder direction $J_\perp$ is much larger than that parallel to the ladder $J_\parallel$ (see scheme 5).

The most significant and unexpected effect of the impurity doping can be seen at low temperatures. While the $\chi_p T$ value for the $x = 0$ crystal increases below 40 K because of the ferromagnetic interaction in the p-EPYNN chain, those for the solid solutions show an opposite tendency: $\chi_p T$ decreases below 40 K. This tendency is enhanced with an increase in x. The doping of non-magnetic [Au(dmit)$_2$] results in the antiferromagnetic behaviour at low temperatures. In order to clarify the origin of this behaviour, the AC susceptibilities χ_{AC} for the solid solutions were recorded in the temperature range down to 50 mK. The results are shown in figure 17, where $\chi_{\mathrm{AC}} T$ are plotted as a function of temperature. The $\chi_{\mathrm{AC}} T$ value for the $x = 0$ material increases with a decrease in temperature, and, after making a maximum at *ca.* 1 K, it shows a decrease, which is probably due to an antiferromagnetic coupling between the ferromagnetic p-EPYNN chains through the diamagnetic [Ni(dmit)$_2$] spin ladder. On the other hand, the $\chi_{\mathrm{AC}} T$ values for the solid solutions of $x = 0.1$, 0.25 and 0.5

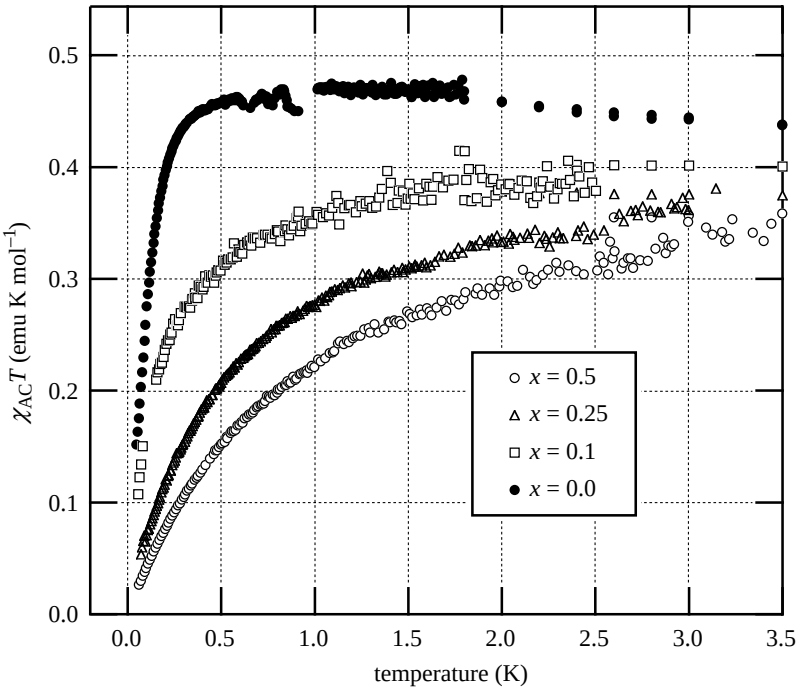

Figure 17. Temperature dependence of the AC susceptibilities χ_{AC} for p-EPYNN $\cdot$ $[Ni(dmit)_2]_{1-x} \cdot [Au(dmit)_2]_x$.

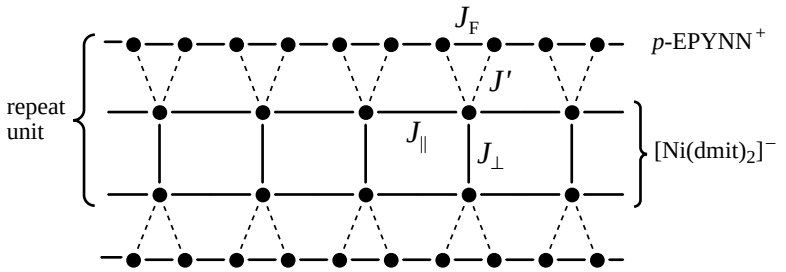

Scheme 5.

monotonically decrease and approach zero at absolute zero. It is reasonably concluded that the p-EPYNN radicals are involved in the antiferromagnetic properties. There should be an enhanced interchain interaction between the ferromagnetic chains of p-EPYNN, and/or an antiferromagnetic intrachain interaction in the p-EPYNN chain.

Scheme 5 represents the magnetic system in the material. The spin ladder of $[Ni(dmit)_2]$ is sandwiched by the chains of p-EPYNN. One $[Ni(dmit)_2]$ molecule interacts with two p-EPYNNs. The parameter J_F is a ferromagnetic coupling constant in the p-EPYNN chain, while $J_\parallel$ and $J_\perp$ are antiferromagnetic couplings in the $[Ni(dmit)_2]$ ladder. The parameter J' represents the interaction between p-EPYNN and $[Ni(dmit)_2]$, and could be antiferromagnetic. When $[Ni(dmit)_2]$ forms a strong singlet pair at the regular sites, J' is negligibly small. However, the antiferromagnetic

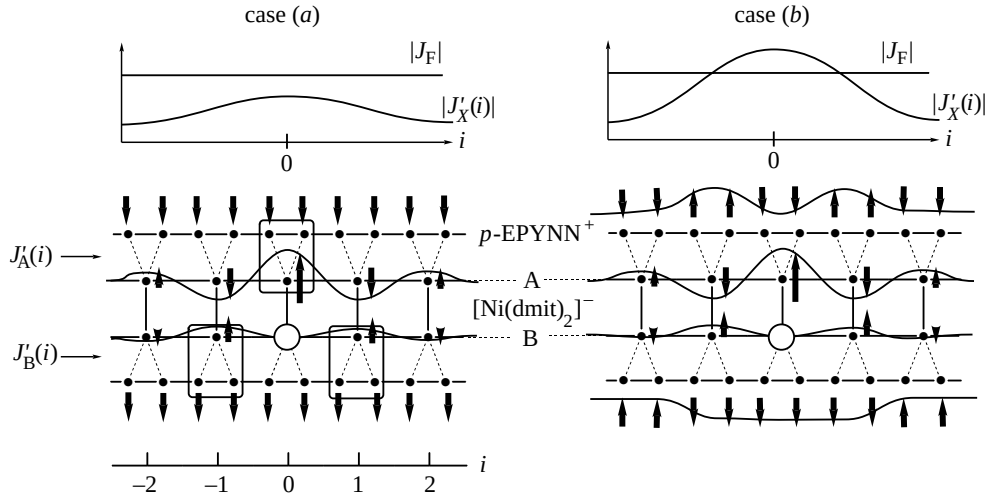

Scheme 6.

property induced by the impurity indicates an enhancement of the antiferromagnetic interaction at the impurity site. The intermolecular arrangements between *p*-EPYNN and $[Ni(dmit)_2]$ are almost the same at the regular and the impurity site, but there should be different J' to understand the observation. Fukuyama *et al*. (1996) studied the impurity effects to the spin ladders theoretically and predicted a spin polarization around the impurity site. Since this idea is widely accepted, it is reasonable to assume a spin density distribution on the molecular spin ladder, as shown in scheme 6. In this case, we can define the pairwise coupling constants between the spin on *p*-EPYNN and the polarized spin on $[Ni(dmit)_2]$, $J'_X(i)$, where i represents the site number and X represents the leg, A or B. It is expected that $J'_X(i)$ is site dependent: it exhibits a maximum at the impurity site and decreases when going far from $i = 0$. Now we think about the relative intensity between $|J_F|$ and $|J'_X(i)|$. If $|J_F|$ is always larger than $|J'_X(i)|$ (case (*a*) in scheme 6), the paramagnetic lattice defect operates as a magnetic coupler between the ferromagnetic *p*-EPYNN chains. The strongest coupling on the leg-A side appears at $i = 0$, while the strongest coupling on the B side appears at $i = -1$ and 1. By assuming local antiferromagnetic coupling between *p*-EPYNN and the polarized spin on $[Ni(dmit)_2]$, the magnetic coupling between the *p*-EPYNN chains is concluded to be ferromagnetic. Since the paramagnetic lattice defects operate as a ferromagnetic coupler, this model cannot explain the observed behaviour. On the other hand, if $|J_F| < |J'_X(i)|$ around the impurity site (case (*b*) in scheme 6), the spin polarization in the spin ladder is transferred into the organic radical chain through the pairwise magnetic interactions, and an antiferromagnetic domain is induced in the *p*-EPYNN chain. This can be regarded as a 'template' effect, and reasonably explains the experimental results.

(*d*) *Summary*

The crystal structures and the magnetic properties of *p*-EPYNN · $[Ni(dmit)_2]$ and *p*-EPYNN · $[Au(dmit)_2]$ were studied. The crystal of *p*-EPYNN · $[Ni(dmit)_2]$ included the ladder structure of $[Ni(dmit)_2]$ sandwiched by the ferromagnetic chain

of *p*-EPYNN. The magnetic measurements concluded the spin gap for the spin ladder. *p*-EPYNN · $[Au(dmit)_2]$ was not isomorphous to *p*-EPYNN · $[Ni(dmit)_2]$, but their structures had interesting similarity. We prepared the solid solutions *p*-EPYNN · $[Ni(dmit)_2]_{1-x} \cdot [Au(dmit)_2]_x$ with $0 \leqslant x \leqslant 0.5$, in which the spin ladder structure was maintained. The doping of the non-magnetic impurity resulted in Curie defects, which suggested $|J_\perp| \gg |J_\parallel|$ in the ladder. The antiferromagnetic behaviour observed at low temperatures was interpreted in terms of the template effect: the spin polarization around the impurity in the ladder was transferred into the *p*-EPYNN chain and resulted in the antiferromagnetic domains.

4. Concluding remarks

We reported the two novel low-dimensional molecule-based magnets, *m*-MPYNN · X and *p*-EPYNN · $[Ni(dmit)_2]$. It was found that they exhibited spin-gap ground states, though there was a big difference between their gap intensities. We speculate that their spin gap states originate in their common characters.

(i) Their structures allow appearance of the RVB states.

(ii) Three-dimensional antiferromagnetic ordering is unstable in them, because of the spin frustration in *m*-MPYNN · X and because of the low dimensionality of the magnetic system in *p*-EPYNN · $[Ni(dmit)_2]$.

In general, the molecule-based magnetic materials exhibit low-dimensional structures that are flexible enough to allow lattice distortions, such as dimerization. They are advantageous to formation of spin-gap ground states, rather than three-dimensional antiferromagnetic states. Low-dimensional molecule-based magnetic materials are quite useful in elucidating the spin-gap states and the RVB states.

We thank our co-workers (Masao Ogata, Tsunehisa Okuno, Akira Yamaguchi, Morikuni Hasegawa, Masahiro Yoshimaru, Wataru Fujita, Takeo Otsuka, Masao Ogata, Hideo Yano, Tatsuya Kobayashi, Seiko Ohira, Hiroyuki Imai) for their important contributions to the works reported herein.

References

Akita, T., Mazaki, Y., Kobayashi, K., Koga, N. & Iwamura, H. 1995 *J. Org. Chem.* **60**, 2092.

Anderson, P. W. 1963 *Magnetism* (ed. G. T. Rado & H. Suhl), vol. 1, p. 25. New York: Academic.

Anderson, P. W. 1973 *Mater. Res. Bull.* **8**, 153.

Awaga, K. & Maruyama, Y. 1989 *Chem. Phys. Lett.* **158**, 556.

Awaga, K., Sugano, T. & Kinoshita, M. 1987 *Chem. Phys. Lett.* **141**, 540.

Awaga, K., Inabe, T., Nagashima, U. & Maruyama, Y. 1989 *J. Chem. Soc. Chem. Commun.*, p. 1617.

Awaga, K., Inabe, T. & Maruyama, Y. 1992*a* *Chem. Phys. Lett.* **190**, 349.

Awaga, K., Inabe, T., Nakamura, T., Matsumoto, M. & Maruyama, Y. 1992*b* *Chem. Phys. Lett.* **195**, 21.

Awaga, K., Yokoyama, T., Fukuda, T., Masuda, S., Harada, Y., Maruyama, Y. & Sato, N. 1993 *Mol. Cryst. Liq. Cryst.* **232**, 27.

Awaga, K., Okuno, T., Yamaguchi, A., Hasegawa, M., Inabe, T., Maruyama, Y. & Wada, N. 1994*a* *Phys. Rev.* B **49**, 3975.

Awaga, K., Yamaguchi, A., Okuno, T., Inabe, T., Nakamura, T., Matsumoto, M. & Maruyama, Y. 1994*b* *J. Mater. Chem.* **4**, 1377.

Azuma, M., Hiroi, Z., Takano, M., Ishida, K. & Kitaoka, Y. 1994 *Phys. Rev. Lett.* **73**, 3463.

Baker Jr, G. A., Rushbrooke, G. S. & Gilbert, H. E. 1964 *Phys. Rev.* A **135**, 1272.

Benelli, C., Caneschi, A., Gatteschi, D. & Sessoli, R. 1993 *Inorg. Chem.* **32**, 4797.

Brewer, J. H., Kreitzman, S. R., Noakes, D. R., Ansaldo, E. J., Harshman, D. R. & Keitel, R. 1986 *Phys. Rev.* B **33**, 7813.

Brossard, L., Ribault, M., Bousseau, M., Valade, L. & Cassoux, P. 1986 *C. R. Acad. Sci. Paris* **302**, 205.

Brossard, L., Hurdequint, H., Ribault, M., Valade, L., Legros, J.-P. & Cassoux, P. 1988 *Synth. Met.* B **27**, 157.

Brossard, L., Ribault, M., Valade, L. & Cassoux, P. 1989 *J. Physique* **50**, 1521.

Bulaevskii, L. N. 1969 *Sov. Phys. Solid State* **11**, 921.

Caneschi, A., Gatteschi, D., Rey, P. & Sessoli, R. 1988 *Inorg. Chem.* **27**, 1756.

Caneschi, A., Gatteschi, D., Renard, J. P., Rey, P. & Sessoli, R. 1989 *Inorg. Chem.* **28**, 2940.

Chandra, P. & Coleman, P. 1991 *Phys. Rev. Lett.* **66**, 100.

Cirujeda, J., Ochando, L. E., Amigó, J. M., Rovira, C., Rius, J. & Veciana, J. 1995 *Angew. Chem. Int. Ed. Engl.* **34**, 55.

D'Anna, J. A. & Wharton, J. H. 1970 *J. Chem. Phys.* **53**, 4047.

Davis, M. S., Morukuma, K. & Kreilick, R. W. 1972 *J. Am. Chem. Soc.* **94**, 5588.

Day, P. 1993 *Science* **261**, 431.

de Panthou, F. L., Luneau, D., Laugier, J. & Rey, P. 1993 *J. Am. Chem. Soc.* **115**, 9095.

Dunsiger, S. R. (and 13 others) 1996 *Phys. Rev.* B **54**, 9091.

Estner, N., Singh, R. & Young, A. P. 1993 *Phys. Rev. Lett.* **71**, 1629.

Fazekas, P. & Anderson, P. W. 1974 *Phil. Mag.* **30**, 423.

Fukuyama, H., Nagaosa, N., Saito, M. & Tanimoto, T. 1996 *J. Phys. Soc. Japan* **65**, 2377.

Gatteschi, D., Laugier, J., Rey, P. & Zanchini, C. 1987 *Inorg. Chem.* **26**, 938.

Haldene, F. D. M. 1983 *Phys. Lett.* A **93**, 464.

Hasegawa, M., Yamaguchi, A., Okuno, T. & Awaga, K. 1995 *Synth. Met.* **71**, 1797.

Hernàndez, E., Mas, M., Molins, E., Rovira, C. & Veciana, J. 1993 *Angew. Chem. Int. Ed. Engl.* **32**, 882.

Imai, H., Inabe, T., Otsuka, T., Okuno, T. & Awaga, K. 1996 *Phys. Rev.* B **54**, 6838.

Inoue, K. & Iwamura, H. 1993 *Chem. Phys. Lett.* **207**, 551.

Jacobs, I. S., Bray, J. W., Hart Jr, H. R., Interrante, L. V., Kasper, J. S. & Watkins, G. D. 1976 *Phys. Rev.* B **14**, 3036.

Johnston, D. C., Johnson, J. W., Goshorn, D. P. & Jacobson, A. J. 1987 *Phys. Rev.* B **35**, 219.

Keren, A., Le, L. P., Luke, G. M., Wu, W. D., Uemura, Y. J., Ajiro, Y., Asano, T., Huriyama, H., Mekata, M. & Kikuchi, H. 1994 *Hyperfine Interactions* **85**, 181.

Keren, A., Kojima, K., Le, L. P., Luke, G. M., Wu, W. D., Uemura, Y. J., Takano, M., Dabkowska, H. & Gingras, N. J. P. 1996 *Phys. Rev.* B **53**, 6451.

Kinoshita, M., Turek, P., Tamura, M., Nozawa, K., Shiomi, D., Nakazawa, Y., Ishikawa, M., Takahashi, M., Awaga, K., Inabe, T. & Maruyama, Y. 1991 *Chem. Lett.*, p. 1225.

Kirmse, R., Stach, J., Dietzsch, W., Steimecke, G. & Hoyer, E. 1980 *Inorg. Chem.* **19**, 2679.

Kittel, C. 1947 *Phys. Rev.* **71**, 270.

Kittel, C. 1948 *Phys. Rev.* **73**, 155.

Kobayashi, A., Kim, H., Sasaki, Y., Kato, R., Kobayashi, H., Moriyama, S., Nishio, Y., Kajita, K. & Sasaki, W. 1987 *Chem. Lett.*, p. 1819.

Kobayashi, A., Kobayashi, H., Miyamoto, A., Kato, R., Clark, R. A. & Underhill, A. E. 1991 *Chem. Lett.*, p. 2163.

Kobayashi, A., Bun, K., Naito, T., Kato, R. & Kobayashi, H. 1992 *Chem. Lett.*, p. 1909.

Komatsu, T., Kojima, N. & Saito, G. 1997 *Solid State Commun.* **103**, 519.

McConnell, H. M. 1967 *Proc. R. A. Welch Found. Chem. Res.* **11**, 144.

Maruta, G., Takeda, S., Yamaguchi, A., Okuno, T., Awaga, K. & Yamaguchi, K. 1999 *Mol. Cryst. Liq. Cryst.* (In the press.)

Matsushita, M. M., Izuoka, A., Sugawara, T., Kobayashi, T., Wada, N., Takeda, N. & Ishikawa, M. 1997 *J. Am. Chem. Soc.* **119**, 4369.

Mekata, M. 1990 *J. Magn. Magn. Mater.* **90/91**, 247.

Nakamura, T. & Miyashita, S. 1995 *Phys. Rev.* B **52**, 9174.

Okuno, T., Otsuka, T. & Awaga, K. 1995 *J. Chem. Soc. Chem. Commun.*, p. 827.

Otsuka, T., Okuno, T., Ohkawa, M., Inabe, T. & Awaga, K. 1997 *Mol. Cryst. Liq. Cryst.* **306**, 285.

Otsuka, T., Okuno, T., Awaga, K. & Inabe, T. 1998 *J. Mater. Chem.* **8**, 1157.

Ramirez, A. P. J. 1991 *Appl. Phys.* **70**, 5952.

Ressouche, E., Boucherle, J., Gillon, B., Rey, P. & Schweizer, J. 1993 *J. Am. Chem. Soc.* **115**, 3610.

Rice, T. M., Gopalan, S. & Sigrist, M. 1994 *Europhys. Lett.* **23**, 445.

Richards, P. M. & Salamon, M. B. 1974 *Phys. Rev.* B **9**, 32.

Rovira, C. (and 12 others) 1997 *Angew. Chem. Int. Ed. Engl.* **36**, 2324.

Siqueira, M., Nyki, J., Cowan, B. & Saunders, J. 1997 *Phys. Rev. Lett.* **76**, 1884.

Stump, H. O., Ouahab, L., Pei, Y., Grandjean, D. & Kahn, O. 1993 *Science* **261**, 447.

Sugano, T., Tamura, M., Kinoshita, M., Sakai, Y. & Ohashi, Y. 1992 *Chem. Phys. Lett.* **200**, 235.

Sugawara, T., Matsushita, M. M., Izuoka, A., Wada, N., Takeda, N. & Ishikawa, M. 1994 *J. Chem. Soc. Chem. Commun.*, p. 1723.

Syozi, I. 1951 *Prog. Theor. Phys.* **6**, 306.

Tajima, H., Inokuchi, M., Kobayashi, A., Ohta, T., Kato, R., Kobayashi, H. & Kuroda, H. 1993 *Chem. Lett.*, p. 1235.

Takeda, K. & Awaga, K. 1997 *Phys. Rev.* B **56**, 14 560.

Takui, T., Miura, Y., Inui, K., Teki, Y., Inoue, M. & Itoh, K. 1995 *Mol. Cryst. Liq. Cryst.* **271**, 55.

Tamura, M., Shiomi, D., Hosokoshi, Y., Iwasawa, N., Nozawa, K., Kinoshita, M., Sawa, H. & Kato, R. 1993 *Mol. Cryst. Liq. Cryst.* **232**, 45.

Togashi, K., Imachi, R., Tomioka, K., Tsuboi, H., Ishida, T., Nogami, T., Takeda, N. & Ishikawa, M. 1996 *Bull. Chem. Soc. Japan* **69**, 2821.

Troyer, M., Tsunetsugu, H. & Würtz, D. 1994 *Phys. Rev.* B **50**, 13 515.

Turek, P., Nozawa, K., Shiomi, D., Awaga, K., Inabe, T., Maruyama, Y. & Kinoshita, M. 1991 *Chem. Phys. Lett.* **180**, 327.

Uemura, Y. J., Yamazaki, T., Harshman, D. R., Senba, M. & Ansaldo, E. J. 1985 *Phys. Rev.* B **31**, 546.

Uemura, Y. J. (and 11 others) 1994 *Phys. Rev. Lett.* **73**, 3306.

Wada, N., Kobayashi, T., Yano, H., Okuno, T., Yamaguchi, A. & Awaga, K. 1997 *J. Phys. Soc. Japan* **66**, 961.

Wang, H., Zhang, D., Wan, M. & Zhu, D. 1993 *Solid State Commun.* **85**, 685.

Wen, X. G., Wilczek, F. & Zee, A. 1989 *Phys. Rev.* B **39**, 11 413.

Wills, A. S. & Harrison, A. 1996 *J. Chem. Soc. Faraday Trans.* **92**, 2161.

Yamaguchi, K., Fueno, T., Nakasuji, K. & Iwamura, H. 1986 *Chem. Lett.*, p. 629.

Yamaguchi, A., Okuno, T. & Awaga, K. 1996 *Bull. Chem. Soc. Japan* **69**, 875.

Zheludev, A., Barone, V., Bonnet, M., Delley, B., Grand, A., Ressouche, E., Rey, P., Subra, R. & Schweizer, J. 1994 *J. Am. Chem. Soc.* **116**, 2019.

Discussion

M. Verdaguer (*Chimie des Metaux de Transition, Université Pierre et Marie Curie, Paris, France*). In Professor Awaga's spin-ladder systems, the ferromagnetic interactions are very weak. He proposes a sophisticated model to explain the magnetic behaviour of the doped system. How can he be sure that under doping, the structure is not changed and hence that the ferromagnetic interactions are maintained?

K. Awaga. (p-EPYNN)[Ni(dmit)$_2$] and (p-EPYNN)[Au(dmit)$_2$] crystallize into different structures. However, the structures of p-EPYNN in them are very similar: p-EPYNN exhibits a side-by-side, head-to-tail one-dimensional stacking. It is, therefore, natural to assume that the structure of p-EPYNN is maintained in the solid solutions, (p-EPYNN)[Ni(dmit)$_2$]$_{(1-x)}$[Au(dmit)$_2$]$_x$.

We studied the magnetic properties of

(p-EPYNN)[Ni(dmit)$_2$],
(p-EPYNN)[Au(dmit)$_2$],
(p-EPYNN)[Ni(dmit)$_2$]$_{(1-x)}$[Au(dmit)$_2$]$_x$

($x > 0.1$). We found that p-EPYNN exhibited ferromagnetic behaviour in the former two but exhibited antiferromagnetic behaviour in the last one. We proposed that paramagnetic lattice defects in the [Ni(dmit)$_2$]$_{(1-x)}$[Au(dmit)$_2$]$_x$ change the magnetic coupling in the p-EPYNN chain from ferromagnetic to antiferromagnetic.